

3.4	Dealing with Measurement Errors and their Effect on the Parameter Recovery	27
3.5	The Impact of Deviations of the Data from the Idealized qDF	33
3.6	The Implications of Assuming a Potential Model which Differs from the Real Potential	38
4	Discussion and Summary	41
4.1	Improved Computational Speed for Application to Larger Data Sets	41
4.2	Modelling Sensitivity to Properties and Unaccounted Imperfections of the Data Set	46
4.3	Data Deviations from the Modelling Assumptions about the Distribution Function and the Paper	
4.4	Different Modelling Approaches using Action-based Distribution Functions	49
4.5	On the Assumption of Axisymmetry	50
5	Acknowledgments	51
A	Appendix	52
A.1	Influence of wrong assumptions about incompleteness of the data parallel to the Galactic plane	
2	Stuff that still needs to be done or thought about	57

1. Introduction

Stellar dynamical modelling is the fundamental tool to infer the gravitational potential of the Milky Way from the positions and motions of its stars (Rix & Bovy 2013; Binney 2011b; Binney & Tremaine 2008) [TO DO: other / better references???]. The observational information on the phase-space coordinates of stars are currently growing at a rapid pace, and will be taken to a whole new level by the upcoming Gaia data. Yet, rigorous and practical modelling tools that turn this information into constraints both on the gravitational potential and on the distribution function (DF) of stellar orbits, are scarce (Rix & Bovy 2013) [TO DO: more references] [TO DO: References that explain that the modelling is scarce, or previous modelling approaches???

Accurately determining the Galactic gravitational potential is fundamental for understanding its dark matter and baryonic structure [TO DO: REF]. Accurately determining the stellar-population dependent orbit distribution function is a fundamental constraint on the

Summary of Comments on DynamicsPaper1_draft_v2.02.pdf

Page: 3

Author: rix Subject: Polygon	Date: 30.08.15 13:37:18
This reads like the intro to a book, or thesis. The basic elements are there, and should be there. We should just perhaps be a bit more sparing with "far-reaching", "fundamenta;" etc..	
Author: rix Subject: Polygonal Line	Date: 30.08.15 13:33:10
Author: rix Subject: Inserted Text	Date: 30.08.15 13:34:30
Author: rix Subject: Inserted Text	Date: 30.08.15 13:33:25
Author: rix Subject: Inserted Text	Date: 30.08.15 13:33:40
Author: rix Subject: Cross-Out	Date: 30.08.15 13:33:42
Author: rix Subject: Inserted Text	Date: 30.08.15 13:33:59
Author: rix Subject: Inserted Text	Date: 30.08.15 13:35:00
Author: rix Subject: Inserted Text	Date: 30.08.15 13:34:15
Author: rix Subject: Cross-Out	Date: 30.08.15 13:35:52
Author: rix Subject: Inserted Text	Date: 30.08.15 13:36:29
Author: rix Subject: Inserted Text	Date: 30.08.15 13:37:29
Author: rix Subject: Inserted Text	Date: 30.08.15 13:38:10

Galaxy's formation history.

Open questions about the MW's potential and structure, on which future modelling attempts will hopefully give more definite answers are: What is the local dark matter density (Zhang et al. 2013; Bovy & Tremaine 2012)? Is the Milky Way's dark matter halo flattened ([TO DO: REF])? Is the MW disk maximal (Sackett 1997) and, to be able to disentangle halo and disk contribution (Dehnen & Binney 1998), what is the disk's overall mass scale length (Bovy & Rix 2013)?

Open questions about the star's distribution within the MW, which dynamical modelling can help to constrain, are: How are stellar kinematics and their chemical abundances are related (Sanders & Binney 2015) [TO DO: REF])? In particular, does the disk have a thin/thick disk dichotomy (Gilmore & Reid 1983) or is it a continuum of many exponential disks (Bovy et al. 2012d)? How does radial migration affect the orbit distribution (Sellwood & Binney 2002; Roškar et al. 2008a,b; Schönrich & Binney 2008; Minchev et al. 2011) [TO DO: These are References from Rix & Bovy 2013 - should I use all of them?]? To address these questions, observed stellar positions and motions need to be turned into full orbits - which stresses again the importance of having a reliable model for the MW's gravitational potential.

In the era of big Galactic surveys all of this could soon be within our reach. Not only will there be full 6D stellar phase-space coordinates for a thousand million of stars measured by Gaia (Perryman et al. 2001) to unprecedented precision by the end of 2016. But already with existing surveys (e.g., SEGUE (Beers et al. 2006), RAVE (Steinmetz et al. 2006), LAMOST (Newberg et al. 2012), APOGEE (Majewski 2012), Gaia-ESO (Gilmore et al. 2012), GALAH (Freeman 2012) [TO DO: I just copied this from Melissa Cannon paper. Should I reference all of them??? Not in reference list yet.]) and sophisticated machine learning tools (e.g. *The Cannon* by Ness et al. (2015)) to combine them, we will soon have huge data sets at our disposal.

In this work we present a rigorous, robust and reliable dynamical modelling machinery, strongly building on previous work by Binney & McMillan (2011); Binney (2012); Bovy & Rix (2013); Bovy (2015) and explicitly developed to exploit and deal with these large data sets in the future.

There is a variety of practical approaches to dynamical modelling of discrete collisionless tracers, such as the stars in the Milky Way (e.g. Jeans modelling; Büdenbender et al. (2015);

Author: rix Subject: Polygonal Line Date: 30.08.15 13:38:10

Author: rix Subject: Cross-Out Date: 30.08.15 13:40:58

Author: rix Subject: Line Date: 30.08.15 13:42:30
This paragraph is good, but 'too soon'

Author: rix Subject: Sticky Note Date: 30.08.15 13:41:51
There is a very strong emphasis (so far) on "local" references.

Loebman et al. (2012); action-based DF modelling: Bovy & Rix (2013); Piffl et al. (2014); Sanders & Binney (2015); torus modelling: Made-to-measure modelling: McMillan & Binney (2012, 2013), De Lorenzi et al. (2007); Syer & Tremaine (1996); Bissantz et al. (2004) or Hunt & Kawata (2014); ~~[TO DO: What kind of modelling is Xiangxiang doing?]; Xue et al. (2015))~~. Most of them – explicitly or implicitly – describe the stellar distribution through a distribution function. Actions are good ways to describe orbits, because they are canonical variables with their corresponding angles, have immediate physical meaning, and obey adiabatic invariance (Binney & Tremaine 2008; McMillan & Binney 2008; Binney 2010; Binney & McMillan 2011; Binney 2011b).

Recently, Binney (2012) and Bovy & Rix (2013) [TO DO: are these the correct references??] proposed to combine parametrized axisymmetric potentials with DF's that are simple analytic functions of the three orbital actions to model discrete data. Binney (2010) and Binney & McMillan (2011) had proposed a set of simple action-based (quasi-isothermal) distribution functions (qDF). Ting et al. (2013) and Bovy & Rix (2013) showed that these qDF's may be good descriptions of the Galactic disk, when one only considers so-called mono-abundance populations (*MAP*), i.e. sub-sets of stars with similar $[\text{Fe}/\text{H}]$ and $[\alpha/\text{Fe}]$ (Bovy et al. 2012b,c,d).

Bovy & Rix (2013) implemented a modelling approach that put action-based DF modelling of the Galactic disk in an axisymmetric potential in practice. Given an assumed potential and an assumed DF, they directly calculated the likelihood of the observed (\vec{x}, \vec{v}) for each sub-set of *MAP* among SEGUE Gdwarf (Yanny et al. 2009). This modelling also accounted for the complex, but known selection function of the kinematic tracers. For each *MAP*, the modelling resulted in a constraint of its DF, and an independent constraint on the gravitational potential, which members of all *MAP*s feel the same way. Taken as an ensemble, the individual *MAP* models constrained the disk surface mass density over a wide range of radii ($\sim 4 - 9$ kpc), and proved a powerful constraint on the disk mass scale length (~ 2 kpc) and on the disk to dark matter ratio at the Solar radius [TO DO: quote number???].

Yet, these recent models still leave us poorly prepared with the wealth and quality of the existing and upcoming data sets. This is because Bovy & Rix (2013) made a number of quite severe and idealizing assumptions about the potential, the DF and the knowledge of observational effects (such as the selection function). All these idealizations are likely to translate into systematic error on the inferred potential or DF, well above the formal error

bars of the upcoming data sets.

In this work we present *RoadMapping* ("Recovery of the Orbit Action Distribution of Mono-Abundance Populations and Potential Inference for our Galaxy") an improved and refined version of the original modelling machinery by Bovy & Rix (2013), making extensive use of the *galpy* python package (Bovy 2015). *RoadMapping* relaxes some of the restraining assumptions Bovy & Rix (2013) ~~had to~~ made, is more flexible and more adept in dealing with large data sets. In this paper we set out to explore the robustness of *RoadMapping* against the breakdowns of some of the most important assumptions of DF-based dynamical modelling. **What is it about the data, the model and the machinery itself that limits our recovery of the true gravitational potential?**

In the light of ~~Gaia~~ we explicitly analyze how well **the modelling machinery** behaves in the limit of large data. For a huge number of stars three ~~statistical~~ aspects become important, that ~~are~~ hidden behind Poisson noise for smaller data sets: (i) We have to make sure that our modelling is an un-biased ~~and asymptotically normal estimator~~ (§3.1). (ii) Numerical inaccuracies in the actual modelling machinery ~~start to matter and need to be avoided~~ (§2.5). (iii) Parameter estimates become so precise ~~that we start to be able to distinguish between similar models. We therefore~~ want more flexibility and more free fit parameters in the potential and DF model. The modelling machinery itself needs to be flexible and fast in effectively finding the best fit parameters for a large set of parameters. The improvements made to the machinery used in Bovy & Rix (2013) are presented in §2.6.

~~Different characteristics of the data might influence the success of the parameter recovery.~~ (i) In an era where we can choose data from different MW surveys, it might be worth to explore if different regions within the MW (i.e. differently shaped or positioned survey volumes) are especially diagnostic to recover the potential (§3.2). (ii) What happens if our knowledge about the selection function, specifically the completeness of the data set within the survey volume, is ~~not perfect~~ (§3.3)? (iii) How to account for measurement errors in the modelling (§3.4)?

One of the strongest assumptions is to restrict the dynamical modelling to a certain family of parametrized models. We investigate how well we can hope to recover the true potential, when our potential and DF models ~~deviate from~~ the true potential and DF. For the DF we specifically investigate two of our assumptions in §3.5: First, what would happen if the stars within MAPs do intrinsically not follow a single qDF as assumed by Ting et al.

Page: 6

	Author: rix Subject: Inserted Text	Date: 31.08.15 08:15:20
	explores and	
	Author: rix Subject: Cross-Out	Date: 31.08.15 08:15:24
	Author: rix Subject: Highlight	Date: 31.08.15 08:16:08
	This sentence, just stands by itself, and seems a bit out of context	
	Author: rix Subject: Cross-Out	Date: 31.08.15 08:16:52
	Author: rix Subject: Highlight	Date: 31.08.15 08:17:25
	If you introduce the term RoadMapping, use it, whenever applicable.	
	Author: rix Subject: Inserted Text	Date: 31.08.15 08:16:36
	the whisker	
	Author: rix Subject: Inserted Text	Date: 31.08.15 08:16:49
	data,	
	Author: rix Subject: Cross-Out	Date: 31.08.15 08:17:45
	Author: rix Subject: Inserted Text	Date: 31.08.15 08:18:02
	may be	
	Author: rix Subject: Cross-Out	Date: 31.08.15 08:18:40
	Unbiased, yes, but why does it have to be asymptotically normal?	
	Author: rix Subject: Inserted Text	Date: 31.08.15 08:19:23
	must not be an important source of systematics	
	Author: rix Subject: Inserted Text	Date: 31.08.15 08:19:36
	As p	
	Author: rix Subject: Inserted Text	Date: 31.08.15 08:20:17
	we need	
	Author: rix Subject: Cross-Out	Date: 31.08.15 08:22:07
	Author: rix Subject: Inserted Text	Date: 31.08.15 08:22:05
	We also explore how different aspects of the observational experiment design impact	
	Author: rix Subject: Inserted Text	Date: 31.08.15 08:22:45
	systematically imperfect	
	Author: rix Subject: Inserted Text	Date: 31.08.15 08:22:50
	best	
	Author: rix Subject: Inserted Text	Date: 31.08.15 08:36:25
	individual	
	Author: rix Subject: Inserted Text	Date: 31.08.15 08:38:09
	do not encompass	

(2013); Bovy & Rix (2013). ~~Second, and assuming MAPs do indeed follow the χ^2 DF, what would be the effect of pollution of MAPs through stars from neighbouring MAPs in the $([Fe/H], [a/Fe])$ plane due to too big abundance errors or bin sizes.~~ And last but not least, we test in §3.6 how well the modelling works, if our assumed potential family deviates from the true potential.

For all of these aspects we show some plausible and illustrative examples on the basis of investigating mock data. The mock data is generated from galaxy models presented in §2.1-2.3 following the procedure in §2.4, analysed according to the description of the machinery in §2.5-2.6 and the results are presented in §3 and discussed in §4.

The strongest assumption that goes into this kind of dynamical modelling might be the idealization of the Galaxy to be axi-symmetric and being in steady state. We do not investigate this within the scope of this paper but strongly suggest a systematic investigation of this for future work.

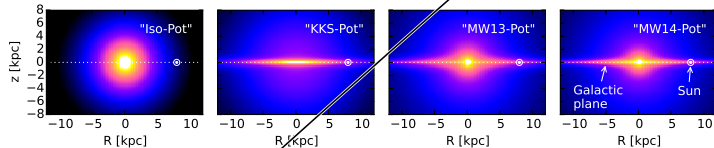


Fig. 1.— Density distribution of the four reference galaxy potentials in Table 1, for illustration purposes. These potentials are used throughout this work for mock data creation and potential recovery. [TG DO: Halo sichtbarer machen, evtl. mit isodensity contours]

Author: rix Subject: Cross-Out Date: 31.08.15 08:38:56
that can come in the main part.

Author: rix Subject: Cross-Out Date: 31.08.15 08:38:58

Author: rix Subject: Inserted Text Date: 31.08.15 08:39:03
Second,

Author: rix Subject: Sticky Note Date: 31.08.15 08:54:56
You might want to look at other paper's introduction: a standard part is the roadmap for the paper for the paper as a whole: In Section 2 we ..., while in Section 3 we ..., Section 4 finally ...

2. Dynamical Modelling

2.1. Actions and Potential Models

Actions. Orbits in axisymmetric potentials are best described and fully specified by the three actions J_R, J_z and $J_\phi = L_z$. They are integrals of motion and generally defined as

$$J_i = \frac{1}{2\pi} \int_{\text{orbit}} p_i(t) dx_i(t) \quad (1)$$

and depend on the potential via the connection between position x_i and momentum p_i along the orbit. Actions have a clear physical meaning: They quantify the amount of oscillation in each coordinate direction of the full orbit [R14]. The position of a star along the orbit is denoted by a set of angles, which form together with the angles a set of canonical conjugate phase-space coordinates [Binney & Tremaine 2008]. Even though actions are the optimal choice as orbit labels and arguments for stellar distribution functions, their computation is very expensive.

Action calculation. The action calculation depends on the choice of potential in which the star moves. The spherical isochrone (Binney & Tremaine 2008) is the only potential for which Equation (1) takes an analytic form. For axisymmetric Stäckel potentials actions can be calculated exactly by the (numerical) evaluation of a single integral. In all other potentials numerically calculated actions will always be approximations, unless Equation (1) is integrated up to infinity. A computational fast way to get actions for arbitrary axisymmetric potentials is the "Stäckel fudge" by Binney (2012), which locally approximates the potential by a Stäckel potential. To speed up the calculation even more, an interpolation grid for J_R and J_z in energy E , angular momentum L_z and [TO DO: what else??] can be build out of these Stäckel fudge actions, as described in Bovy (2015).¹

Potential models. In our modelling we assume a family of parametrized potentials with a fixed number of free parameters. We use different kinds of potentials: Besides the Milky Way like potential from Bovy & Rix (2013) ("MW13-Pot") with bulge, disk and halo, we also extensively use the spherical isochrone potential ("Iso-Pot") in our test suites to make use of the analytic (and therefore exact and fast) way to calculate actions. In addition we use the 2-component Kuzmin-Kutuzov Stäckel potential by Batsleer & Dejonghe (1994) ("KKS-Pot"), which displays a disk and halo structure and also provides exact actions. Table 1

¹[TO DO: Write which numerical accuracy I needed for the grid, as the default values were not good enough.]

Author: rix Subject: Sticky Note Date: 02.09.15 09:11:03

Give a 1-2 sentence intro to the Section. E.g.

In this Section, we summarize the basic elements of the dynamical modelling presented here, which in many respects follows BR14.

Author: rix Subject: Cross-Out Date: 02.09.15 09:13:42

Author: rix Subject: Inserted Text Date: 02.09.15 09:11:30

Author: rix Subject: Inserted Text Date: 02.09.15 09:51:26

Author: rix Subject: Inserted Text Date: 02.09.15 09:11:43

Author: rix Subject: Inserted Text Date: 02.09.15 09:11:48

Author: rix Subject: Polygonal Line Date: 02.09.15 09:14:55

Author: rix Subject: Polygonal Line Date: 02.09.15 09:14:09

Author: rix Subject: Inserted Text Date: 02.09.15 09:34:52

Author: rix Subject: Cross-Out Date: 02.09.15 09:48:54

Author: rix Subject: Inserted Text Date: 02.09.15 09:36:21

Author: rix Subject: Inserted Text Date: 02.09.15 09:36:35

Author: rix Subject: Inserted Text Date: 02.09.15 09:36:43

Author: rix Subject: Inserted Text Date: 02.09.15 09:37:10

Author: rix Subject: Inserted Text Date: 02.09.15 09:38:27

Author: rix Subject: Inserted Text Date: 02.09.15 09:39:22

Author: rix Subject: Cross-Out Date: 02.09.15 09:41:29

Author: rix Subject: Inserted Text Date: 02.09.15 09:41:43

Author: rix Subject: Inserted Text Date: 02.09.15 09:42:20

summarizes all reference potentials together used in this work with their free parameters $p\Phi$. The density distribution of these potentials is illustrated in Figure 1.

2.2. Distribution Function

Distribution Function. Motivated by the findings of Bovy et al. (2012b,c,d) and Ting et al. (2013) about the simple phase space structure of MAPs, and following Bovy & Rix (2013) and their successful application, we also assume that each MAP follows a single qDF of the form given by Binney & McMillan (2011). This qDF is a function of the actions $\mathbf{J} = (J_R, J_z, L_z)$ and has the form

$$\begin{aligned} \text{qDF}(\mathbf{J} \mid p_{\text{DF}}) \\ = f_{\sigma_R}(J_R, L_z \mid p_{\text{DF}}) \times f_{\sigma_z}(J_z, L_z \mid p_{\text{DF}}) \end{aligned} \quad (2)$$

with

$$\begin{aligned} f_{\sigma_R}(J_R, L_z \mid p_{\text{DF}}) = n \times \frac{\Omega}{\pi \sigma_R^2(R_g) \kappa} \exp\left(-\frac{\kappa J_R}{\sigma_R^2(R_g)}\right) \\ \times [1 + \tanh(L_z/L_0)] \end{aligned} \quad (3)$$

$$f_{\sigma_z}(J_z, L_z \mid p_{\text{DF}}) = \frac{\nu}{2\pi \sigma_z^2(R_g)} \exp\left(-\frac{\nu J_z}{\sigma_z^2(R_g)}\right) \quad (4)$$

$$(5)$$

Here $R_g \equiv R_g(L_z)$ and $\Omega \equiv \Omega(L_z)$ are the (guidig-center) radius and the circular frequency of the circular orbit with angular momentum L_z in a given potential. $\kappa \equiv \kappa(L_z)$ and $\nu \equiv \nu(L_z)$ are the radial/epicycle (κ) and vertical (ν) frequencies with which the star would oscillate around the circular orbit in R - and z -direction when slightly perturbed (Binney & Tremaine 2008). The term $[1 + \tanh(L_z/L_0)]$ suppresses counter-rotation for orbits in the disk with $L \gg L_0$ which we set to a random small value ($L_0 = 10 \times R_\odot / 8 \times v_{\text{circ}}(R_\odot) / 220$).

For this qDF to be able to incorporate the findings by Bovy et al. (2012b,b,c) about the phase space structure of MAPs summarized in §1, we set the functions n , σ_R and σ_z , which indirectly set the stellar number density and radial and vertical velocity dispersion profiles,

$$n(R_g \mid p_{\text{DF}}) \propto \exp\left(-\frac{R_g}{h_R}\right) \quad (6)$$

$$\sigma_R(R_g \mid p_{\text{DF}}) = \sigma_{R,0} \times \exp\left(-\frac{R_g - R_\odot}{h_{\sigma,R}}\right) \quad (7)$$

$$\sigma_z(R_g \mid p_{\text{DF}}) = \sigma_{z,0} \times \exp\left(-\frac{R_g - R_\odot}{h_{\sigma,z}}\right). \quad (8)$$

Author: rix Subject: Inserted Text	Date: 02.09.15 09:45:33
Star	
Author: rix Subject: Inserted Text	Date: 02.09.15 09:45:34
s	
Author: rix Subject: Inserted Text	Date: 02.09.15 09:50:35
This is m	
Author: rix Subject: Polygonal Line	Date: 02.09.15 09:50:25
Author: rix Subject: Inserted Text	Date: 02.09.15 09:49:28
Throughout, we assume	
Author: rix Subject: Inserted Text	Date: 02.09.15 09:49:51
the orbits of	
Author: rix Subject: Inserted Text	Date: 02.09.15 09:50:02
can be described	
Author: rix Subject: Cross-Out	Date: 02.09.15 10:00:51
Author: rix Subject: Sticky Note	Date: 02.09.15 09:53:27
(end of sentence)	
Author: rix Subject: Sticky Note	Date: 02.09.15 09:59:26
In all BT08 reference, mention subsection.	
Author: rix Subject: Cross-Out	Date: 02.09.15 10:02:24
Author: rix Subject: Inserted Text	Date: 02.09.15 10:00:46
To match the observed properties of MAPs	
Author: rix Subject: Cross-Out	Date: 02.09.15 10:03:18
Author: rix Subject: Inserted Text	Date: 02.09.15 10:02:34
(see	
Author: rix Subject: Inserted Text	Date: 02.09.15 10:02:59
Choose the functional forms	

The qDF for each MAP has therefore a set of five free parameters p_{DF} : the density scale length of the tracers h_R , the radial and vertical velocity dispersion at the solar position R_\odot , $\sigma_{R,0}$ and $\sigma_{z,0}$, and the scale lengths $h_{\sigma,R}$ and $h_{\sigma,z}$, that describe the radial decrease of the velocity dispersion. The MAPs we use for illustration through out this work are summarized in Table 2.



Tracer Density. One crucial point in our dynamical modelling technique (§2.5), as well as in creating mock data (§2.4), is to calculate the (axisymmetric) spatial tracer density $\rho_{\text{DF}}(\mathbf{x} | p_\Phi, p_{\text{DF}})$ for a given qDF and potential. We do this by integrating the qDF at a given (R, z) over all three velocity components, using a N_{velocity} -th order Gauss-Legendre quadrature for each integral:

$$\begin{aligned} \rho_{\text{DF}}(R, |z| | p_\Phi, p_{\text{DF}}) &= \int_{-\infty}^{\infty} \int_{-\infty}^{\infty} \int_{-\infty}^{\infty} \text{qDF}(J[R, z, \mathbf{v} | p_\Phi] | p_{\text{DF}}) d^3\mathbf{v} \end{aligned} \quad (9)$$

$$\approx \int_{-N_{\text{sigma}}\sigma_R(R|p_{\text{DF}})}^{N_{\text{sigma}}\sigma_R(R|p_{\text{DF}})} \int_{-N_{\text{sigma}}\sigma_z(R|p_{\text{DF}})}^{N_{\text{sigma}}\sigma_z(R|p_{\text{DF}})} \int_0^{1.5v_{\text{circ}}(R_\odot)} \text{qDF}(J[R, z, \mathbf{v} | p_\Phi] | p_{\text{DF}}) dv_T dv_z dv_R \quad (10)$$

where $\sigma_R(R | p_{\text{DF}})$ and $\sigma_z(R | p_{\text{DF}})$ are given by Equations (7) and (8) and the integration ranges are motivated by Figure 2. The integration range $[0, 1.5v_{\text{circ}}(R_\odot)]$ over v_T is in general sufficient (only for observation volumes at smaller Galactocentric radii with larger velocities this upper limit needs to be increased). For a given p_Φ and p_{DF} we explicitly calculate the density on $N_{\text{spatial}} \times N_{\text{spatial}}$ regular grid points in the (R, z) plane; in between grid points the density is evaluated with a bivariate spline interpolation. The grid is chosen to cover the extent of the observations for $z > 0$. The total number of actions that need to be calculated to set up the density interpolation grid is $N_{\text{spatial}}^2 \cdot N_{\text{velocity}}^3$. §2.5 and Figure 3 show the importance of choosing N_{spatial} , N_{velocity} and N_{sigma} sufficiently large in order to get the density with an acceptable numerical accuracy.

2.3. Selection Function

Galactic Coordinate System. Our modelling takes place in the Galactocentric rest-frame with cylindrical coordinates $\mathbf{x} \equiv (R, \phi, z)$ and corresponding velocity components $\mathbf{v} \equiv (v_R, v_\phi, v_z)$. If the stellar phase-space data is given in observed coordinates, position $\mathbf{x} \equiv (\alpha, \delta, m - M)$ in right ascension α , declination δ and distance modulus $(m - M)$, and velocity $\mathbf{v} \equiv (\mu_\alpha, \mu_\delta, v_{\text{los}})$ as proper motions $\boldsymbol{\mu} \equiv (\mu_\alpha, \mu_\delta)$ [TO DO: cos somewhere??] and

Author: rix Subject: Sticky Note Date: 02.09.15 10:04:13	
In this section, you have so indicate somehow, where you recapitulate BR13, and what is added new.	
Author: rix Subject: Line Date: 02.09.15 10:05:55	
Author: rix Subject: Line Date: 02.09.15 10:06:00	
Author: rix Subject: Line Date: 02.09.15 10:05:49	
Author: rix Subject: Polygonal Line Date: 02.09.15 10:05:30	
Author: rix Subject: Highlight Date: 02.09.15 10:09:04	
Why z>0? Is it not symmetric in z, by construction?	
Author: rix Subject: Highlight Date: 02.09.15 10:09:32	
This seems out of place here: move to the beginning of the paragraph.	

line-of-sight velocity v_{los} , the data (\mathbf{x}, \mathbf{v}) has to be converted first into the Galactocentric rest-frame coordinates (\mathbf{x}, \mathbf{v}) using the sun's position and velocity. For simplicity we assume for the sun

$$\begin{aligned} (R_{\odot}, \phi_{\odot}, z_{\odot}) &= (8 \text{ kpc}, 0^{\circ}, 0 \text{ kpc}) \\ (v_{R,\odot}, v_{T,\odot}, v_{z,\odot}) &= (0, 230, 0) \text{ km s}^{-1}. \end{aligned}$$

Selection Function. A survey's selection function can be understood as a subvolume in the space of observables: e.g. position on the plane of the sky (limited by the pointing of the survey), distance from the sun (limited by the brightness of the stars and the sensitivity of the detector), colors and metallicity of the stars (limited by survey mode and targeting). Within the framework of this paper, using only mock data for testing purposes, we ignore target cuts in colors and metallicity and simply use spatial selection functions, which we define as

$$\text{sf}(\mathbf{x}) \equiv \begin{cases} \text{completeness}(\mathbf{x}) & \text{if } \mathbf{x} \text{ within observed volume} \\ 0 & \text{outside} \end{cases}$$

Its value describes the probability to observe a star at \mathbf{x} .

For the observed volume we use simple geometrical shapes: Either a sphere of radius r_{max} with the sun at its center, or a "wedge", which we define as the angular segment of an cylindrical annuli, i.e. the volume with $R \in [R_{\text{min}}, R_{\text{max}}]$, $\phi \in [\phi_{\text{min}}, \phi_{\text{max}}]$, $z \in [z_{\text{min}}, z_{\text{max}}]$ within the model galaxy. The sharp outer cut of the survey volume could be understood as the detection limit in apparent brightness in the case, where all stars have the same luminosity.

The completeness is, in our framework, a function of position with $0 \leq \text{completeness}(\mathbf{x}) \leq 1$ everywhere inside the observed volume. It could be understood as a position-dependent detection probability. Unless explicitly stated otherwise, we use everywhere

$$\text{completeness}(\mathbf{x}) = 1.$$

2.4. Mock Data

One goal of this work is to test how the loss of information in the process of measuring stellar phase space coordinates can affect the outcome of the modelling. To investigate this, we assume first that our measured stars do indeed come from our assumed families of

Author: rix Subject: Highlight	Date: 02.09.15 10:09:09
Author: rix Subject: Line	Date: 02.09.15 10:10:10
Author: rix Subject: Inserted Text	Date: 02.09.15 10:11:29
Author: rix Subject: Inserted Text	Date: 02.09.15 10:16:45
Author: rix Subject: Cross-Out	Date: 02.09.15 10:20:47
Author: rix Subject: Inserted Text	Date: 02.09.15 10:20:53
Author: rix Subject: Cross-Out	Date: 02.09.15 10:25:12
Author: rix Subject: Inserted Text	Date: 02.09.15 10:22:36
Author: rix Subject: Polygonal Line	Date: 02.09.15 10:26:03
Author: rix Subject: Cross-Out	Date: 02.09.15 10:26:15
Author: rix Subject: Cross-Out	Date: 02.09.15 10:25:18
Author: rix Subject: Inserted Text	Date: 02.09.15 11:30:47
Author: rix Subject: Inserted Text	Date: 02.09.15 11:31:22
Author: rix Subject: Cross-Out	Date: 02.09.15 11:32:21
Author: rix Subject: Inserted Text	Date: 02.09.15 11:34:36
Author: rix Subject: Cross-Out	Date: 02.09.15 11:35:01
Author: rix Subject: Inserted Text	Date: 02.09.15 11:34:57
Author: rix Subject: Cross-Out	Date: 02.09.15 11:35:26
Author: rix Subject: Polygonal Line	Date: 02.09.15 11:35:44
Author: rix Subject: Inserted Text	Date: 02.09.15 11:35:22
Author: rix Subject: Inserted Text	Date: 02.09.15 14:53:35

potentials and distribution functions and draw mock data from a given true distribution. In further steps we can manipulate and modify these mock data sets to mimick observational effects.

The distribution function is given in terms of actions and angles. The transformation $(J_i, \theta_i) \rightarrow (x_i, v_i)$ is however difficult to perform and computationally much more expensive than the transformation $(x_i, v_i) \rightarrow (J_i, \theta_i)$. We propose a fast and simple two step method for drawing mock data from an action distribution function, which also accounts effectively for a given survey selection function.

Preparation: Tracer density. We first setup the interpolation grid for the tracer density $\rho(R, |z| | p_\Phi, p_{DF})$ generated by the given qDF and according to §2.2 and Equation (10). For the creation of the mock data we use $N_{\text{spatial}} = 20$, $N_{\text{velocity}} = 40$ and $N_{\text{sigma}} = 5$.

Step 1: Drawing positions from the selection function. To get positions \mathbf{x} , for our mock data stars, we first sample random positions (R_i, z_i, ϕ_i) uniformly from the observed volume. Then we apply a rejection Monte Carlo method to these positions using the pre-calculated $\rho_{DF}(R, |z| | p_\Phi, p_{DF})$. In an optional third step, if we want to apply a non-uniform selection function, $\text{sf}(\mathbf{x}) \neq \text{const.}$ within the observed volume, we use the rejection method a second time. The sample then follows

$$\mathbf{x}_i \rightarrow p(\mathbf{x}) \propto \rho_{DF}(R, z | p_\Phi, p_{DF}) \times \text{sf}(\mathbf{x}).$$

Step 2: Drawing velocities according to the distribution function. The velocities are independent of the selection function and observed volume. For each of the positions (R_i, z_i) we now sample velocities directly from the qDF $(R_i, z_i, \mathbf{v} | p_{Phi}, p_{DF})$ using a rejection method. To reduce the number of rejected velocities, we use a Gaussian in velocity space as an envelope function, from which we first randomly sample velocities and then apply the rejection method to shape the Gaussian velocity distribution towards the velocity distribution predicted by the qDF. We now have a mock data set according to the required:

$$(x_i, v_i) \rightarrow p(\mathbf{x}, \mathbf{v}) \propto \text{qDF}(\mathbf{x}, \mathbf{v} | p_\Phi, p_{DF}) \times \text{sf}(\mathbf{x}).$$

Example: Figure 2 shows examples of mock data sets in configuration space (\mathbf{x}, \mathbf{v}) and action space. The qDF represents realistic stellar distributions in position-velocity space. More stars are found at smaller R and $|z|$, and are distributed uniformly in ϕ according to our assumption of axisymmetry. The distribution in radial and vertical velocities, v_R and v_z , is approximately Gaussian with the (total projected) velocity dispersion being $\sim \sigma_{R,0}$

Author: rix Subject: Inserted Text	Date: 02.09.15 14:54:06
Subsequently,	
Author: rix Subject: Polygonal Line	Date: 02.09.15 14:57:47
Author: rix Subject: Cross-Out	Date: 02.09.15 14:55:44
Author: rix Subject: Inserted Text	Date: 02.09.15 14:56:23
space	
Author: rix Subject: Inserted Text	Date: 02.09.15 14:58:41
within the entire observable	
Author: rix Subject: Inserted Text	Date: 02.09.15 14:59:06
to	
Author: rix Subject: Polygonal Line	Date: 02.09.15 15:00:11
Author: rix Subject: Inserted Text	Date: 02.09.15 14:59:42
resulting	
Author: rix Subject: Inserted Text	Date: 02.09.15 15:00:34
within the	
Author: rix Subject: Inserted Text	Date: 02.09.15 15:01:44
satisfying	
Author: rix Subject: Polygonal Line	Date: 02.09.15 15:01:57
Author: rix Subject: Cross-Out	Date: 02.09.15 15:02:25
Author: rix Subject: Inserted Text	Date: 02.09.15 15:05:48
The mock data from the	
Author: rix Subject: Inserted Text	Date: 02.09.15 15:06:25
lead to the expected distributions in configuration space	

and $\sim \sigma_{z,0}$ (see Table 2). The distribution of tangential velocities v_T is skewed because of asymmetric drift [TO DO: Find out, if we need an explanation for asymmetric drift here]. The distribution in action space demonstrates the intuitive physical meaning of actions: The stars of the "cool" MAP have in general lower radial and vertical actions, as they are on more circular orbits. The different relative distributions of the radial and vertical actions J_R and J_z of the "hot" and "cool" MAP is due to them having different velocity anisotropy $\sigma_{R,0}/\sigma_{z,0}$. The different ranges of angular momentum L_z in the two volumes reflect $L_z \sim R v_{\text{circ}}$ and the different radial extent of both volumes. The volume above the plane contains more stars with higher J_z , because stars with small J_z can't reach that far above the plane. Circular orbits with $J_R = 0$ and $J_z = 0$ can only be observed in the Galactic mid-plane. An orbit with L_z much smaller or larger than $L_z(R_\odot)$ can only reach into a volume located around R_\odot , if it is more eccentric and has therefore larger J_R . This together with the effect of asymmetric drift can be seen in the asymmetric distribution of J_R in the top central panel of Figure 2. [TO DO: Part of this could also be mentioned in the figure caption.]

Introducing measurement errors. If we want to add measurement errors to the mock data, we need to apply two modifications to the above procedure. First, measurement errors are best described in the phase-space of observables. We use the heliocentric coordinate system right ascension and declination (α, δ) and distance modulus $(m - M)$ as proxy for the distance from the sun, the proper motion in both α and δ direction (μ_α, μ_δ) and the line-of-sight velocity v_{los} . For the conversion between these observables and the Galactocentric cylindrical coordinate system in which the analysis takes place, we need the position and velocity of the sun, which we set for simplicity in this study to be $(R_\odot, z_\odot) = (8, 0)$ kpc and $(v_R, v_T, v_z) = (0, 230, 0)$ km s⁻¹. We assume Gaussian measurement errors in the observables $\tilde{\mathbf{x}} = (\alpha, \delta, (m - M))$, $\tilde{\mathbf{v}} = (\mu_\alpha, \mu_\delta, v_{\text{los}})$. Second, in the case of distance errors, stars can virtually scatter in and out of the observed volume. To account for this, we first draw "true" positions from a volume that is larger than the actual observation volume, perturb the stars positions according to the distance errors and then reject all stars that lie now outside of the observed volume. This procedure mirrors the Poisson scatter around the detection threshold for stars whose distances are determined from the apparent brightness and the distance modulus. [TO DO: Can I say it like this????] We then sample velocities (given the "true" positions of the stars) as described above and perturb them according to the measurement errors as well.

Author: rix Subject: Cross-Out	Date: 02.09.15 15:07:31
no, we don't	
Author: rix Subject: Inserted Text	Date: 02.09.15 15:07:45
illustrates	
Author: rix Subject: Highlight	Date: 02.09.15 15:08:11
Did you ever talk about "cool" and "hot" before?	
Author: rix Subject: Cross-Out	Date: 02.09.15 15:09:40
Author: rix Subject: Inserted Text	Date: 02.09.15 15:13:02
cannot	
Author: rix Subject: Cross-Out	Date: 02.09.15 15:16:30
Author: rix Subject: Cross-Out	Date: 02.09.15 15:16:19
You've said that before.	
Author: rix Subject: Inserted Text	Date: 02.09.15 15:16:49
, where we have taken m-M as a proxy for distance.	
Author: rix Subject: Highlight	Date: 02.09.15 15:15:31
Looks good to me.	

2.5. Likelihood

Form of the likelihood. As data we use the positions and velocities of stars coming from a given MAP and survey selection function $\text{sf}(\mathbf{x})$,

$$D = \{\mathbf{x}_i, \mathbf{v}_i \mid \text{(star } i \text{ belonging to same MAP)} \\ \wedge \text{ (sf}(\mathbf{x}_i) > 0)\}$$

The model that we fit to the data is a parametrized potential and a single qDF with a given number of fixed and free parameters,

$$p_M = \{p_{\text{DF}}, p_{\Phi}\},$$

We fit the qDF parameters (see §2.2) with a logarithmically flat prior, i.e. flat priors in

$$p_{\text{DF}} := \{ \ln(h_R/8\text{kpc}), \\ \ln(\sigma_{R,0}/220\text{km s}^{-1}), \ln(\sigma_{z,0}/220\text{km s}^{-1}), \\ \ln(h_{\sigma,R}/8\text{kpc}), \ln(h_{\sigma,z}/8\text{kpc}) \}.$$

The orbit of the i -th star in a potential with p_{Φ} is labeled by the actions $\mathbf{J}_i := \mathbf{J}[\mathbf{x}_i, \mathbf{v}_i \mid p_{\Phi}]$ and the qDF evaluated for the i -th star is then $\text{qDF}(\mathbf{J}_i \mid p_M) := \text{qDF}(\mathbf{J}[\mathbf{x}_i, \mathbf{v}_i \mid p_{\Phi}] \mid p_{\text{DF}})$

The likelihood of the data given the model $\mathcal{L} = (D \mid p_M)$ is the product of the probabilities for each star to move in the potential with p_{Φ} , being within the survey's selection function and it's orbit to be drawn from the qDF with p_{DF} , i.e.

$$\begin{aligned} \mathcal{L}(p_M \mid D) &\equiv \prod_i^N P(\mathbf{x}_i, \mathbf{v}_i \mid p_M) \\ &= \prod_i^N \frac{1}{(r_o v_o)^3} \cdot \frac{\text{qDF}(\mathbf{J}_i \mid p_M) \cdot \text{sf}(\mathbf{x}_i)}{\int d^3x d^3v \text{qDF}(\mathbf{J} \mid p_M) \cdot \text{sf}(\mathbf{x})} \\ &\propto \prod_i^N \frac{1}{(r_o v_o)^3} \cdot \frac{\text{qDF}(\mathbf{J}_i \mid p_M)}{\int d^3x \rho_{\text{DF}}(R, |z| \mid p_M) \cdot \text{sf}(\mathbf{x})}, \end{aligned} \quad (11)$$

where N is the number of stars in the data set D . In the last step we used Equation (9). The factor $\prod_i \text{sf}(\mathbf{x}_i)$ is independent of the model parameters, so we simply evaluate Equation (11) in the likelihood calculation. We find the best set of model parameters by maximising the likelihood.

Author: rix Subject: Inserted Text	Date: 02.09.15 15:21:36
Data	
Author: rix Subject: Cross-Out	Date: 02.09.15 15:21:39
Author: rix Subject: Inserted Text	Date: 02.09.15 15:22:37
consider here	
Author: rix Subject: Inserted Text	Date: 02.09.15 15:25:25
is specified by a	
Author: rix Subject: Inserted Text	Date: 02.09.15 15:25:30
for the	
Author: rix Subject: Inserted Text	Date: 02.09.15 15:25:50
Author: rix Subject: Inserted Text	Date: 02.09.15 15:26:26
we assume a prior that is flat in	
Author: rix Subject: Sticky Note	Date: 08.09.15 08:05:44
If the prior is flat, then you don't need the normalizations (8kpc etc.), and everything fits on one line.	
Author: rix Subject: Cross-Out	Date: 08.09.15 08:07:06
these quantities have been defined previously, no?	
Author: rix Subject: Sticky Note	Date: 08.09.15 08:11:42
what happened to sf(x_i) in the numerator of the last step? Correct or explain?	
Author: rix Subject: Sticky Note	Date: 08.09.15 08:12:17
B.t.w: Equation 9 and 10 are ONE equation... shouldn't give it two numbers	
Author: rix Subject: Inserted Text	Date: 02.09.15 15:27:39
, and in	

A word on units. We evaluate the likelihood in a scale-free potential within a Galactocentric coordinate system which is defined as $v_{\text{circ}}(R=1) = 1$. The circular velocity at the sun's radius, $v_{\text{circ}}(R_{\odot} \sim 8 \text{ kpc}) \sim 230 \text{ km s}^{-1}$, determines the total mass amplitude of the galaxy potential. In the modelling all data and model parameters are re-scaled to spatial units of $r_o := R_{\odot}$ or velocity units of $v_o := v_{\text{circ}}(R_{\odot})$. The prefactor $1/(r_o v_o)^3$ in Equation (11) makes sure that the likelihood has the correct units to satisfy:

$$\int P(\mathbf{x}, \mathbf{v} | p_M) d^3x d^3v \propto 1$$

Including this prefactor is crucial when $v_{\text{circ}}(R_{\odot})$ is a free fitting parameter.

Numerical accuracy in calculating the likelihood. The normalisation in Equation (11) is a measure for the total number of tracers inside the survey volume,

$$M_{\text{tot}} \equiv \int d^3x \rho_{\text{DF}}(R, |z| | p_{\text{model}}) \cdot \text{sf}(\mathbf{x}). \quad (12)$$

In the case of an axisymmetric galaxy model and $\text{sf}(\mathbf{x}) = 1$ everywhere inside the observed volume (i.e. a complete sample as assumed in most tests in this work), the normalisation is essentially a two-dimensional integral in R and z of the interpolated tracer density ρ_{DF} . See Equation (10) and surrounding text) over the survey volume, times the observation volume's geometric angular contribution at each (R, z) . We perform this integral as a Gauss Legendre quadrature of order 40 in each R and z direction. Unfortunately, the evaluation of the likelihood for only one set of model parameters is computationally expensive. The computation speed is set by the number of action calculations required, i.e. the number of stars and the numerical accuracy of the integrals in Equation (10) needed for the normalisation, which requires $N_{\text{spatial}}^2 \times N_{\text{velocity}}^3$ action calculations. The accuracy has to be chosen high enough, such that a resulting numerical error

$$\delta M_{\text{tot}} \equiv \frac{M_{\text{tot}}(N_{\text{spatial}}, N_{\text{velocity}}, N_{\text{signature}}) - M_{\text{tot, true}}}{M_{\text{tot, true}}} \quad (13)$$

does not dominate the likelihood, i.e.

$$\begin{aligned} & \log \mathcal{L}(p_M | D) \\ &= \sum_i^N \log \text{qDF}(\mathbf{J}_i | p_M) - 3N \log(r_o v_o) \\ & \quad - N \log(M_{\text{tot, true}}) - N \log(1 + \delta M_{\text{tot}}), \end{aligned} \quad (14)$$

Author: rix Subject: Polygon	Date: 08.09.15 08:15:23
I think you need to use two different symbols, because else it is unclear what units v_circ has. In you first use here it has units of [1] in the second instant it has units of [km/s]. Use \tilde{v}ide that or something for the velocities and distances that have unit [1].	
Author: rix Subject: Polygonal Line	Date: 08.09.15 08:16:34
Author: rix Subject: Highlight	Date: 08.09.15 08:18:56
Not sure I understand this: isn't it just the differential Volume. The "angular contribution" seems not well defined (to me)	
Author: rix Subject: Polygonal Line	Date: 08.09.15 08:20:57
Author: rix Subject: Inserted Text	Date: 08.09.15 08:20:08
It turns out that the sufficiently	
Author: rix Subject: Inserted Text	Date: 08.09.15 08:21:11
even for	
Author: rix Subject: Inserted Text	Date: 08.09.15 08:21:47
This expense is dominated	
Author: rix Subject: Inserted Text	Date: 08.09.15 08:22:33
which in turn depends on	
Author: rix Subject: Inserted Text	Date: 08.09.15 08:22:41
in the sample	
Author: rix Subject: Polygon	Date: 08.09.15 08:24:08
There are many equations that seem needlessly split into two lines, for reasons that are not clear to me. Please try to put as many equations back into the most compact way to write them. Either within the text, or just one line.	
Author: rix Subject: Cross-Out	Date: 08.09.15 08:25:50
Author: rix Subject: Inserted Text	Date: 08.09.15 08:25:31
estimated	
Author: rix Subject: Polygon	Date: 08.09.15 08:27:15
This, too, can fit on one line	
Author: rix Subject: Cross-Out	Date: 08.09.15 08:26:06

with

$$N \log(1 + \delta_{M_{tot}}) \lesssim 1.$$

In other words, this error is only small enough, if it does not affect the comparison of two adjacent models whose likelihoods differ, to be clearly distinguishable, by a factor of 10 . Otherwise numerical inaccuracies could lead to systematic biases in the potential and MCMC fitting. For data sets as large as $N = 20,000$ stars in one MAP, which in the age of GAIA could very well be the case [TO DO: Really???], ~~we would need~~ a numerical accuracy of 0.005% in the normalisation. Figure 3 demonstrates that the numerical accuracy we use in the analysis, $N_{\text{spatial}} = 16$, $N_{\text{velocity}} = 24$ and $N_{\text{syma}} = 5$, does satisfy this requirement.

Dealing with measurement errors. We assume Gaussian errors in the observable space $\mathbf{y} \equiv (\bar{\mathbf{x}}, \bar{\mathbf{v}}) = (\text{RA}, \text{DEC}, (m - M), \mu_{\text{RA}}, \mu_{\text{DEC}}, v_{\text{los}})$,

$$\begin{aligned} N[\mathbf{y}_i | \delta \mathbf{y}_i](\mathbf{y}') &= N[\mathbf{y}', \delta \mathbf{y}_i](\mathbf{y}_i) \\ &\equiv \prod_k \frac{1}{\sqrt{2\pi(\delta y_{i,k})^2}} \exp\left(-\frac{(y_{i,k} - y'_{i,k})^2}{2(\delta y_{i,k})^2}\right), \end{aligned}$$

where $y_{i,k}$ is the k -th coordinate in \mathbf{y}_i of the i -th star. Observed stars follow the (quasi-isothermal) distribution function ($\text{DF}(\mathbf{y}) \equiv \text{qDF}(\mathbf{J}[\mathbf{y} | p_\Phi] | p_{\text{DF}})$ for short), convolved with the error distribution $N[0, \delta \mathbf{y}](\mathbf{y})$. The selection function $\text{sf}(\mathbf{y})$ acts on the space of (error affected) observables. Then the probability of one star coming from potential p_Φ , distribution function p_{DF} and being affected by the measurement errors $\delta \mathbf{y}$ becomes

$$\begin{aligned} &\tilde{P}(\mathbf{y}_i | p_\Phi, p_{\text{DF}}, \delta \mathbf{y}_i) \\ &\equiv \frac{\text{sf}(\mathbf{y}_i) \cdot \int d^6 \mathbf{y}' \text{DF}(\mathbf{y}') \cdot N[\mathbf{y}_i, \delta \mathbf{y}_i](\mathbf{y}')}{\int d^6 \mathbf{y} \text{DF}(\mathbf{y}) \cdot \int d^6 \mathbf{y}' \text{sf}(\mathbf{y}') \cdot N[\mathbf{y}, \delta \mathbf{y}_i](\mathbf{y}')}. \end{aligned}$$

In the case of errors in distance or position, the evaluation of this is computational expensive - especially if the stars have heteroscedastic errors $\delta \mathbf{y}_i$, for which the normalisation would have to be calculated for each star separately. In practice we apply the following approximation:

$$\begin{aligned} &\tilde{P}(\mathbf{y}_i | p_\Phi, p_{\text{DF}}, \delta \mathbf{y}_i) \\ &\approx \frac{\text{sf}(\mathbf{x}_i)}{\int d^6 \mathbf{y} \text{DF}(\mathbf{y}) \cdot \text{sf}(\mathbf{x})} \cdot \frac{1}{N_{\text{error}}} \sum_n^{N_{\text{error}}} \text{DF}(\mathbf{x}_i, \mathbf{v}[\mathbf{y}'_{i,n}]) \end{aligned} \quad (15)$$

with

$$\mathbf{y}'_{i,n} \sim N[\mathbf{y}_i, \delta \mathbf{y}_i](\mathbf{y}')$$

Author: rix Subject: Polygon	Date: 08.09.15 08:29:13
I would strongly advise against using linear and log likelihoods mixed in "talking" about them. Do you mean DeltaLogLikelihood=1?	
Author: rix Subject: Cross-Out	Date: 08.09.15 08:27:28
Author: rix Subject: Sticky Note	Date: 09.09.15 17:59:48
remember: Gaia will mostly give us motions (and distances), NOT detailed abundances; probably not even a/lFe	
Author: rix Subject: Inserted Text	Date: 09.09.15 17:58:35
one needs	
Author: rix Subject: Sticky Note	Date: 09.09.15 18:00:55
What I am missing in this Section is any distinction of what aspects are "new" (not addressed in existing papers) and what is repatulated to be coherent..	
Author: rix Subject: Inserted Text	Date: 09.09.15 18:00:01
incorporating	
Author: rix Subject: Sticky Note	Date: 09.09.15 18:03:31
I am not sure I understand this notation [...]; also "Y" seems undefined in the text. Why not call it y, as opposed to y_ik	
Author: rix Subject: Highlight	Date: 09.09.15 18:04:04
something is screwy with the parentheses here..	
Author: rix Subject: Cross-Out	Date: 09.09.15 18:04:52

Fig. 3.— (Continued.) We calculate the true normalization with high accuracy as $M_{\text{tot,true}} \approx M_{\text{tot}}(N_{\text{spatial}} = 20, N_{\text{velocity}} = 56, N_{\text{sigma}} = 7)$. The dashed lines indicate the accuracy used in our analyses: it is better than 0.002% for all three potential types. Only for the smallest volume in the "MW13-Pot" (yellow line) the error is only $\sim 0.005\%$. This could be due to the fact, that, while we have analytical formulas to calculate the actions for the isochrone and the Staekel potential exactly, we have to resort to an approximate action calculation for the MW-like potential (see §2.1). [TO DO: Try to redo yellow curve in MW. Weird, that it does not depend on N_{spatial} .??] [TO DO: fancybox Legend]

In doing so, we ignore errors in the star's position \mathbf{x}_i altogether. This simplifies the normalisation drastically and makes it independent of measurement errors, including the velocity errors. Distance errors however are included, but only implicitly in the convolution over the stars' velocity errors in the Galactocentric restframe. We calculate the convolution using Monte Carlo integration with N_{error} samples drawn from the full error Gaussian in observable space, $y'_{i,n}$.

2.6. Fitting Procedure

We search the (p_Φ, p_{DF}) parameter space for the maximum of the likelihood in Equation (11) using a two-step procedure: The first step finds the approximate peak and width of the likelihood using a nested-grid search, while the second step samples the shape of the likelihood (or rather the posterior probability distribution) using a Monte-Carlo Markov Chain (MCMC) approach.

Fitting Step 1: Nested-grid search. The (p_Φ, p_{DF}) parameter space can be high-dimensional. To effectively minimizing the number of likelihood evaluations before finding its peak, we use a nested-grid approach:

- *Initialization.* For N free model parameters $M = (p_\Phi, p_{\text{DF}})$, we set up a sufficiently large initial grid with 3^N regular grid points.
- *Evaluation.* We evaluate the likelihood at each grid-point. Because of the many computationally expensive $\mathbf{x}, \mathbf{v} \xrightarrow{p_\Phi} \mathbf{J}$ transformations that have to be performed for each new set of p_Φ parameters, an outer loop iterates over the p_Φ parameters and precalculates the actions, while an inner loop evaluates the likelihood Equation (11) for all qDF parameters p_{DF} with the actions in the given potential and (analogously to Figure 9 in Bovy & Rix (2013)).

- *Iteration.* To find from the very sparse 3^N likelihood grid a new grid, that is more centered on the likelihood and has a width of order of the width of the likelihood, we proceed as follows: For each of the model parameter in M we marginalize the likelihood by summing over the grid. If the resulting 3 points all lie within 4σ of a Gaussian, we fit a Gaussian to the 3 points and determine a new 4σ fitting range. Otherwise the grid point with the highest likelihood becomes the new fitting range. We proceed with iteratively evaluating the likelihood on finer and finer grids, until we have found a 4-sigma fit range in each of the model parameter dimensions.
- *The fiducial qDF.* For the above strategy to work properly, the action pre-calculations have to be independent of the choice of qDF parameters. This is clearly the case for the $N_j \times N_{\text{error}}$ stellar data actions \mathbf{J}_i . To calculate the normalisation in Equation (11), $N_{\text{spatial}}^2 \times N_{\text{velocity}}^3$ actions \mathbf{J}_n are needed. Formally the spatial coordinates at which the \mathbf{J}_n are calculated depend on the p_{DF} parameters via the integration ranges in Equation (10). To relax this dependence we instead use the same velocity integration limits in the likelihood calculations for all p_{DF} s in a given potential. This set of parameters, that sets the velocity integration range globally, $(\sigma_{p,0}, \sigma_{z,0}, h_{\sigma,R}, h_{\sigma,z})$ in Equation (7) and (8), is referred to as the "fiducial qDF". Using the same integration range in the density calculation for all qDFs at a given p_Φ makes the normalisation vary smoothly with different p_{DF} . Choosing a fiducial qDF that is very off from the true qDF can however lead to large biases. The optimal values for the fiducial qDF are the (yet unknown) best fit p_{DF} parameters. We take care of this by setting, in each iteration step of the nested-grid search, the fiducial qDF simply to the p_{DF} parameters of the central grid point. As the nested-grid search approaches the best fit values, the fiducial qDF approaches automatically the optimal values as well. This is another advantage of the nested-grid search, because the result will not be biased by a poor choice of the fiducial qDF.
- *Speed Limitations.* Overall the computation speed of this nested-grid approach is dominated (in descending order of importance) by a) the complexity of potential and action calculation, b) the number $N_j \times N_{\text{error}} + N_{\text{spatial}}^2 \times N_{\text{velocity}}^3$ of actions to calculate, i.e. the number of stars, error samples and numerical accuracy of the normalisation calculations, c) the number of different potentials to investigate (i.e. the number of free potential parameters and number of grid points in each dimension) and d) the number of qDFs to investigate. The latter is also non-negligible, because for such a large number of actions the number of qDF-function evaluations also take some time.

Fitting Step 2: MCMC. After the nested-grid search is converged, the grid is centered at the peak of the likelihood and its extent contains the 4σ confidence interval. To actually sample the full shape of the likelihood, we could do a grid search with much finer grid spacing (e.g. $K = 11$ in each dimension). The number of grid points scales exponentially with number of free parameters N . For a large number of free parameters ($N > 4$) a Monte Carlo Markov Chain (MCMC) approach might sample the likelihood (or rather the posterior probability distribution, which is the likelihood times some priors, see §????) much faster. We use *emcee* by Foreman-Mackey et al. (2013) and release the walkers very close to the likelihood peak found by the nested-grid search, which will assure fast convergence in much less than K^N likelihood evaluations.

For a sufficiently high numerical accuracy in calculating the integrals in Equation (10) the current qDF parameters as each values can be used as integration ranges. To get reasonable results also for slightly lower accuracy, a single fiducial qDF can be used for all likelihood evaluations within the MCMC as well. As fiducial qDF we use the qDF parameters of the likelihood peak, found by the nested-grid search.

3. Results

We are now in a position to explore the questions about the ultimate limitations of action based modelling, posed in the introduction:

- Can we still retrieve unbiased model parameter estimates p_M in the limit of large sample sizes?
- What role does the survey volume and geometry play, at given sample size?
- What if our knowledge of the sample selection function is imperfect, and potentially biased?
- How do the parameter estimates deteriorate if the individual errors on the phase-space coordinates become significant?

But we also consider the more fundamental limitations:

- What if the observed stars are not exactly drawn from the family of model distribution functions?
- What happens to the estimate of the potential and the DF, if the actual potential is not contained in the family of model potentials?

Author: rix Subject: Inserted Text	Date: 09.09.15 18:20:26
Author: rix Subject: Inserted Text	Date: 09.09.15 18:21:01
Author: rix Subject: Inserted Text	Date: 09.09.15 18:21:05
Author: rix Subject: Sticky Note	Date: 09.09.15 18:23:10
The likelihood (units: per data) and the posterior (units: per parameters) have different units. One can use them almost interchangeably, if one assumed flat priors. We should state the priors to be clear). Here you call it first a likelihood, and then -- as apology -- say, well, it's kind of a posterior.	
Author: rix Subject: Cross-Out	Date: 09.09.15 18:23:33
Author: rix Subject: Polygon	Date: 09.09.15 18:26:50
This has all been said before (intro) and will be addressed return in teh subsequent section; so, no need to spend half a page on it.	
I would just say: the limitations of action based modelling posed in the introduction (unbiased estimates; survey volume; imperfect selection function; measurement errors; actual DF or Phi not spanned by the space of models).	
Author: rix Subject: Cross-Out	Date: 09.09.15 18:23:50
Author: rix Subject: Inserted Text	Date: 09.09.15 18:24:00

We do not explore the breakdown of the assumption that the system is axisymmetric and in steady state. Except of the test suite on measurement errors in §3.4, we assume that the phase-space errors are negligible.

3.1. Model Parameter Estimates in the Limit of Large Data Sets

The individual MAP in Bovy & Rix (2013) contained typically between 100 and 800 objects, so that each MAP implied a quite broad *pdf* for the model parameters $p_M = \{p_\Phi, p_{DF}\}$. Here we explore what happens in the limit of *very* much larger samples for each MAP, say 20,000 objects. As outlined in §2.5 the immediate consequence of larger samples is given by the likelihood normalization requirement, $\log(1 + \text{rel.error}) \leq 1/N_{\text{sample}}$ (see Equation 14), which is the modelling aspect that drives the computing time. This issues aside, we would, however, expect that in the limit of large data sets with vanishing measurement errors the *pdfs* of the p_M become Gaussian, with a *pdf* width (i.e. standard error SE of the Gaussian) that scales as $1/\sqrt{N_{\text{sample}}}$. Further, we must verify that any bias in the *pdf* expectation value is *far* less than SE, even for quite large samples.

Using sets of mock data, created according to §2.4 and *with our* fiducial model for p_M in Table 3, *Tests 3.2, 3.3 and 3.1*, we verified that *RoadMapping* satisfies all these conditions and expectations. Figure 4 illustrates the joint *pdf*'s of all p_M . This figure illustrates that the *pdf*'s are multivariate Gaussians that project into Gaussians when considering the marginalized *pdf* for all the individual p_M . Note that some of the parameters are quite covariant, but the level of their actual covariance depends on the choice of the p_M from which the mock data were drawn. Figure 5 then illustrates that the *pdf* width, SE, indeed scales as $1/\sqrt{N_{\text{sample}}}$. Figure 6 illustrates even more, that *RoadMapping* satisfies the central limit theorem. The average parameter estimates from many mock samples with identical underlying p_M are very close to the input p_M , and the distribution of the actual parameter estimates are a Gaussian around it.

3.2. The Role of the Survey Volume Geometry

Beyond the sample size, the survey volume *per se* must play a role; clearly, even a vast and perfect data set of stars within 100 pc of the Sun, has limited power to tell us about the potential at very different R . Intuitively, having dynamical tracers over a wide range in R suggests to allow tighter constraints on the radial dependence of the potential. To this end, we devise two suites of mock data sets:

	Author: rix Subject: Inserted Text	Date: 09.09.15 18:33:24
	Author: rix Subject: Polygonal Line	Date: 09.09.15 18:27:18
	Author: rix Subject: Cross-Out	Date: 09.09.15 18:33:37
	Author: rix Subject: Highlight	Date: 09.09.15 18:34:44
	Did that child not have a name in Sectin 2.5? 'idolM' _idol)?	
	Author: rix Subject: Inserted Text	Date: 09.09.15 18:49:12
	considerably	
	Author: rix Subject: Inserted Text	Date: 09.09.15 18:50:06
	ine	
	Author: rix Subject: Highlight	Date: 09.09.15 19:55:18
	I don't understand this here: both gramatically and	
	Author: rix Subject: Cross-Out	Date: 15.09.15 11:51:36
	Author: rix Subject: Highlight	Date: 15.09.15 11:51:29
	This is a restatement of the intro; not necessary to repeat here. I do like intro sentences to Sections, but not intro paragraphs.	
	Author: rix Subject: Inserted Text	Date: 15.09.15 11:52:20
	explore the role of the survey volume per se (see intro subsection) at given sample size	

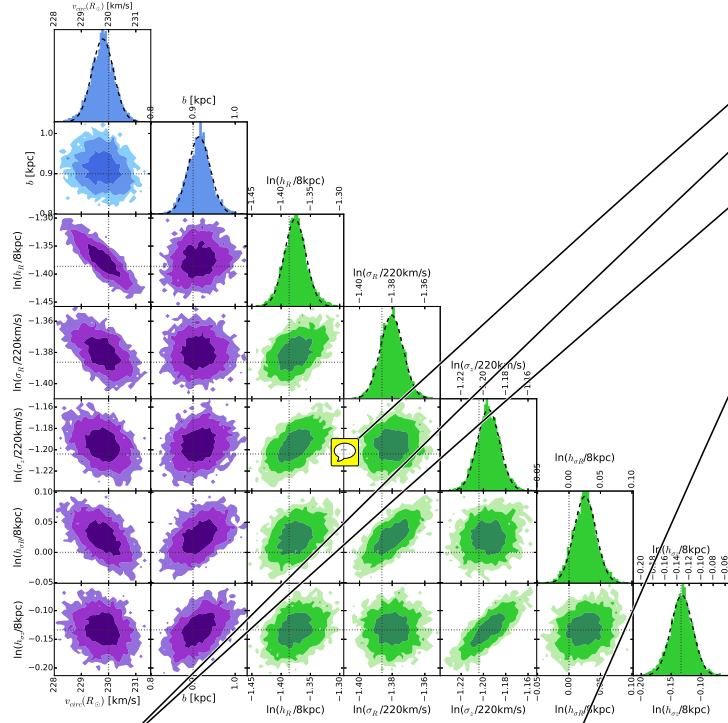


Fig. 4.— The **likelihood** in Equation (11) in the parameter space $p_M = \{p_\Phi, \ln(p_{DF})\}$ for one example mock data set created according to Test 3.1 in Table 3. **Blue** indicates the likelihood for the potential parameters, green the qDF parameters. The true parameters are marked by dotted lines. The dark, medium and bright contours in the 2D distributions represent **1, 2 and 3 sigma confidence regions**, respectively, and show weak or moderate covariances. This analysis was picked among five similar analyses, to have all 1 sigma contours encompass the input values. The likelihood here was sampled using MCMC (with flat priors in p_Φ and $\ln(p_{DF})$ to turn the likelihood into a full *pdf*). Because only 10,000 MCMC samples were used to create the histograms shown, the 2D distribution has noisy contours. The dashed lines in the 1D distributions are Gaussian fits to the histogram of MCMC samples. This demonstrates very well that for such a large number of stars, the likelihood approaches the shape of a multi-variate Gaussian, as expected from the central limit theorem. [TO DO: rename h_{-R} to h_{+R} , σ_R to σ_{R0} and analogous for z]

Author: rix Subject: Sticky Note Date: 15.09.15 11:53:50

Beautiful Figure

Author: rix Subject: Highlight Date: 15.09.15 11:53:37

This looks like a triangle plot done with emcee; MCMC produces, as you state, posterior probabilities ... please make language and nomenclature consistent.

Author: rix Subject: Inserted Text Date: 15.09.15 11:57:20

Purple

Author: rix Subject: Highlight Date: 15.09.15 11:58:13

This is where this matters: is this a confidence on the data or on the parameters?

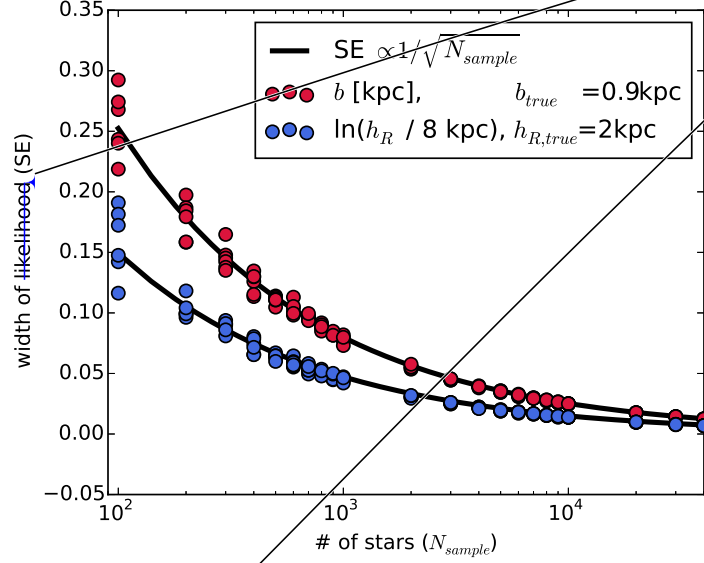


Fig. 5.— The width of the **likelihood** for two fit parameters found from analyses of 132 mock data sets vs. the number of stars in each data set. The mock data was created in the "Iso-Pot" potential and all model parameters are given as Test 3.2 in Table 3. The likelihood in Equation (11) was evaluated on a grid and a Gaussian was fitted to the marginalized likelihoods of each free fit parameter. The standard error (SE) of these best fit Gaussians is shown for the potential parameter b in kpc (red dots) and for the qDF parameter $\ln(h_R/8\text{kpc})$ in dimensionless units (blue). The black lines are fits of the functional form $\text{SE}(N_{\text{sample}}) \propto 1/\sqrt{N_{\text{sample}}}$ to the data points of both shown parameters. As can be seen, for large data samples the width of the likelihood behaves as expected and scales with $1/\sqrt{N_{\text{sample}}}$ as predicted by the central limit theorem. [TO DO: fancybox Legend]

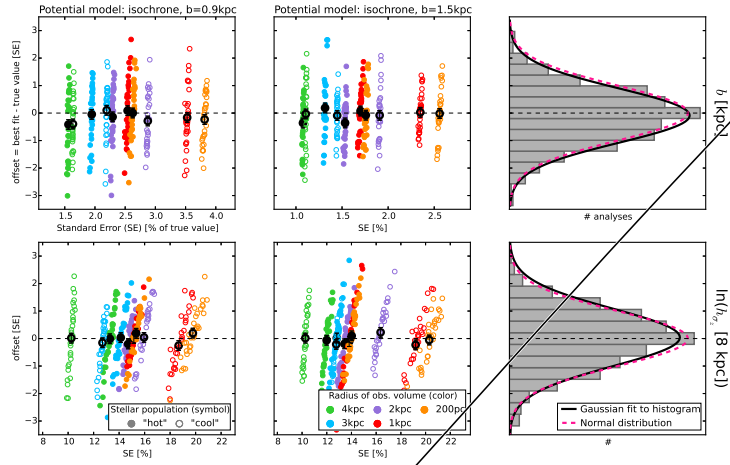


Fig. 6.— (Un-)bias of the parameter estimate: According to the central limit theorem the likelihood will follow a Gaussian distribution for a large number of stars. From this follows that also for a large number of data sets the corresponding best fit values for the model parameters have to follow a Gaussian distribution, centered on the true model parameters. That our method satisfies this and is therefore an unbiased estimator [TO DO: can I say that????] is demonstrated here. We create 640 mock data sets. They come from two different "Iso-Pot" potentials (first and second column), two different stellar populations ("hot" MAP (solid symbols) and "cool" MAP (open symbols)) and five spherical observation volumes of different sizes (color coded, see legend). All model parameters are summarized in Table 3 as Test 3.3. We determine the best fit value and the standard error (SE) for each fit parameter by fitting a Gaussian to the marginalized likelihood. The offset is the difference between the best fit and the true value of each model parameter. In the first two columns the offset in units of the SE is plotted vs. the SE in % of the true model parameter. The first row shows the results for the isochrone scale length b and the second row the qDF parameter $h_{\sigma,z}$, which corresponds to the scale length of the vertical velocity distribution. [TO DO: rename isochrone potential in title to "Iso-Pot".] [TO DO: rename $h_{\sigma R}$ to $h_{\sigma,R}$, σ_R to $\sigma_{R,0}$ and analogous for z]

Fig. 6.— (Continued.) The last column finally displays a histogram of the 640 offsets (in units of the corresponding SE). The black solid line is a Gaussian fit to a histogram. The dashed pink line is a normal distribution $\mathcal{N}(0,1)$. As they agree very well, our modelling method is therefore well-behaved and unbiased. For the 32 analyses belonging to one model we also determine the mean offset and SE, which are overplotted in black in the first two columns (with $1/\sqrt{32}$ as error). [TO DO: Is the scatter of the black symbols too large??? Is the reason for this numerical inaccuracies???] [TO DO: fancybox Legend!]

The first one draws mock data from the same p_M (see Test 4 in Table 3), but from four different volume wedges (see §2.3), illustrated in the right upper panel of Figure 7. To make the parameter inference comparison very differential, the mock data sets are equally large (20,000) in all cases, and are drawn from identical total survey volumes (4.5 kpc^3 , achieved by adjusting the angular width of the edges). We perform the same test for three different potential models ("Iso-Pot", "MW14-Pot" and "KKS-Pot").

The results of this first mock suite are shown in Figure 7 for all potential fit parameters. The mock suite was created to investigate the influence of position and shape of the survey volume within the Galaxy, together with the choice of potential model.

The second suite of mock data sets was already introduced in §3.1 (see also Test 3.3), where mock data sets were drawn from five spherical volumes around the sun with different maximum radius, for two "Iso-Pot"s and two different MAPs.

The results of this second suite are shown in Figure 6 for one potential and one PDF parameter ($\ln(h_{\sigma,z})$) and demonstrate the effect of the size and extent of the survey volume together with the choice of the MAP and model parameters.

The left panels in Figures 6 and 7 illustrate the ability of RoadMapping to constrain model parameters, with the standard error of the pdf as measure of the precision on the x -axis. Figure 6 demonstrates that, given a choice of PDF and potential parameters, a larger volume always results in tighter constraints. There is no obvious trend that a hotter or cooler MAP will always give better results; it depends on the survey volume and the model parameter in question. In Figure 7 the wedges all have the same size and all give results of similar precision. Minor differences, e.g. with the "Iso-Pot" potential being less constrained in the wedge with large vertical, but small radial extent, are a special property of the considered potential and parameters, and not a global property of the corresponding survey volume. In the case of an axisymmetric model galaxy, the extent in ϕ direction is not expected to matter. Overall radial extent and vertical extent seem therefore to be equally important to constrain the potential. In addition Figure 7 implies that for these cases volumes offsets in the radial or vertical direction have at most modest impact - at least at given sample size. While we believe the argument for significant radial and vertical extent is generic, we have

Author: rix Subject: Inserted Text	Date: 15.09.15 11:59:37
Author: rix Subject: Highlight	Date: 15.09.15 12:01:17
Author: rix Subject: Highlight	Date: 15.09.15 12:02:01
Author: rix Subject: Highlight	Date: 15.09.15 12:03:19
Author: rix Subject: Highlight	Date: 15.09.15 12:04:19
Author: rix Subject: Highlight	Date: 15.09.15 12:12:40
Author: rix Subject: Highlight	Date: 15.09.15 12:13:23
Author: rix Subject: Inserted Text	Date: 15.09.15 12:14:00
Author: rix Subject: Inserted Text	Date: 15.09.15 12:14:25
Author: rix Subject: Inserted Text	Date: 15.09.15 12:14:44
Author: rix Subject: Cross-Out	Date: 15.09.15 12:15:01
Author: rix Subject: Inserted Text	Date: 15.09.15 12:15:05

not done a full exploration of all combinations of p_M and volumina.

3.3. The Significance of Incorrect assumptions on the (In-)Completeness of the Data Set

The selection function of a survey could be described by a spatial survey volume and a completeness function, which determines the fraction of stars observed at a given location within the Galaxy with a given brightness, metallicity etc (see §2.3). The completeness function depends on the characteristics and mode of the survey, can be very complex and is therefore sometimes not perfectly known. We investigate how much an imperfect knowledge of the selection function can affect the recovery of the potential. We model this by creating mock data with varying incompleteness, while assuming constant completeness in the analysis. The mock data comes from a sphere around the sun and an incompleteness function that drops linearly with distance r from the sun (see Test 5, Example 1, in Table 3 and Figure 8).

This could be understood as a model for the important effect of stars being less likely to be observed the further away they are. We demonstrate that the potential recovery with *RoadMapping* is very robust against somewhat wrong assumptions about the (in-)completeness of the data (see Figure 9). A lot of information about the potential comes from the rotation curve measurements in the plane, which is not affected by applying an incompleteness function. In Appendix §A.1 we also show that the robustness is somewhat less striking but still given for small misjudgments of the incompleteness in vertical direction, parallel to the disk plane (Figures 19 and 20). This could model the effect of wrong corrections for dust obscuration in the plane. We also investigate in Appendix §A.1 if indeed most of the information is stored in the rotation curve. For this we use the same mock data sets as analysed in Figures 9 and 20, but this time were not including the tangential velocities in the modelling, rather marginalizing the likelihood over v_T . In this case the potential is much less tightly constrained, even for 20,000 stars. For only small deviations of true and assumed completeness ($\lesssim 10\%$) we can however still incorporate the true potential in our fitting result (see Figure 21).

3.4. Dealing with Measurement Errors and their Effect on the Parameter Recovery

Convergence of the error integral. In §2.5 we introduced how we convolve the model probability with the measurement errors. In the absence of distance errors the accuracy of

Author: rix Subject: Inserted Text	Date: 15.09.15 12:15:36
Impact of Misjudging the	
Author: rix Subject: Cross-Out	Date: 15.09.15 12:16:31
Author: rix Subject: Polygonal Line	Date: 15.09.15 12:16:26
Author: rix Subject: Inserted Text	Date: 15.09.15 12:17:10
(within a maximal survey volume)	
Author: rix Subject: Inserted Text	Date: 15.09.15 12:18:06
with	
Author: rix Subject: Inserted Text	Date: 15.09.15 12:18:36
captures the relevant case	
Author: rix Subject: Inserted Text	Date: 15.09.15 12:18:49
(than assumed)	
Author: rix Subject: Inserted Text	Date: 15.09.15 12:19:07
radial	
Author: rix Subject: Inserted Text	Date: 15.09.15 12:20:36
Apparently, much	
Author: rix Subject: Highlight	Date: 15.09.15 12:22:42
I don't have an immediate solution for this, but again, it seems the interesting question of "how much of the information is in the rotation curve" is 'hidden' in the section on selection functions...	
Author: rix Subject: Sticky Note	Date: 15.09.15 12:49:49
This Section has three parts: -- convergence of the integral -- testing the approximation -- underestimating errors	
It seems to me that the basic Section: What is the impact of the errors? Is missing. That should be the center piece, and the other three aspects should be quick summary notes, only 1-2 sentences long.	
Author: rix Subject: Cross-Out	Date: 15.09.15 12:24:15

Fig. 9.— Influence of wrong assumptions about the radial incompleteness of the data on the parameter recovery with *RoadMapping*. Each mock data set was created having different incompleteness parameters ϵ_r (shown on the x -axis and illustrated in Figure 8) and the model parameters are given as Test 5, Example 1, in Table 3. The analysis however didn't know about the incompleteness and assumed that all data sets had constant completeness within the survey volume ($\epsilon_r = 0$). The marginalized likelihoods from the fits are shown as violins. The green lines mark the true potential parameters ("Iso-Pot") and the red and blue lines the true qDF parameters ("hot" MAP in red and "cool" MAP in blue), which we tried to recover. The *RoadMapping* method seems to be very robust against small to intermediate deviations between the true and the assumed data incompleteness. [TO DO: rename $h_{\sigma R}$ to $h_{\sigma,R}$, σ_R to $\sigma_{R,0}$ and analogous for z]

the parameter recovery is limited by an insufficient MC sampling of the convolution integral in Equation (15). Test 6.1 in Table 3 and Figure 10 investigate how many MC samples are needed, given the size of the velocity error, for the integral to be accurate within certain limits:

For each $\delta\mu \in [2, 3, 4, 5]\text{mas yr}^{-1}$ we set up four mock data sets and evaluated the likelihood for different N_{error} . We used $N_{\text{conv}} := 800$ and 1200 MC samples to calculate the numerically converged likelihood for proper motion errors $\delta\mu \leq 3\text{mas yr}^{-1}$ and $\delta\mu > 3\text{mas yr}^{-1}$, respectively (see left panels in Figure 11). We determined the mean bias

$$\text{BIAS}(N_{\text{error}}, \delta\mu) \equiv \frac{1}{4} \sum_{j=1}^4 [\langle p_i \rangle(N_{\text{error}}, \delta\mu)]_j - [\langle p_i \rangle(N_{\text{conv}}, \delta\mu)]_j,$$

where $[\langle p_i \rangle(N_{\text{error}}, \delta\mu)]_j$ is the best estimate for the i -th model parameter $p_i \in p_M$ from the analysis of the j -th mock data realisation with $\delta\mu$ using N_{error} MC samples. From this we then generated the curves $N_{\text{error},i}(\delta v_{\text{max}}, \text{BIAS})$ in Figure 10 by linear interpolation, that show how many MC samples are needed for parameter p_i given a velocity error and a systematic bias in units of the standard error (SE) of the estimate. The proper motion error $\delta\mu$ translates to a velocity error according to

$$\delta v_{\text{max}} [\text{km s}^{-1}] \equiv 4.74047 \cdot r_{\text{max}} [\text{kpc}] \cdot \delta\mu [\text{mas yr}^{-1}], \quad (16)$$

where r_{max} is the maximum distance of stars. We find in Figure 10 the relation

$$N_{\text{error},i}(\delta v_{\text{max}}, \text{BIAS}) \propto (\delta v_{\text{max}})^2.$$

Figure 10 also demonstrates that different model parameters do not have the same sensitivity to the numerical inaccuracies introduced by insufficient sampling. [TO DO: we haven't tested yet, if this plot depends on hotness of population and / or number of stars. But if it takes forever to actually do the calculations, I guess, we just leave it like this.]

Author: rix Subject: Cross-Out Date: 15.09.15 12:25:25

Author: rix Subject: Cross-Out Date: 15.09.15 12:25:33

Author: rix Subject: Inserted Text Date: 15.09.15 12:25:42
pic

Author: rix Subject: Cross-Out Date: 15.09.15 12:26:11

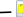



Author: rix Subject: Sticky Note Date: 15.09.15 12:27:25
But I presume you don't assume delta_r_max for ALL stars in the sample?
It's all "heteroskedastic", i.e. delta_v-O-delta_mu...

Testing the error convolved likelihood approximation. In absence of distance (modulus) errors our approximation for the likelihood, which is the model probability convolved with the measurement errors in Equation (15), is equal to the true likelihood. In case there *are* distance modulus errors, this likelihood links the range of possible velocities (specified by the measurement errors in line-of-sight velocity, proper motion and distance modulus) to a fixed but slightly wrong position, as we ignore the distance error in the position. As the link between position and velocity provides the information about the potential, this will lead to systematic biases in the parameter recovery the larger the distance error becomes. In Test 6.2 in Table 3 and Figure 11 we investigate the capabilities of Equation (15) with and without distance modulus errors.

The left column of panels in Figure 11 shows how well the approximation works in the absence of distance errors. There seemed to be no biases in the parameter recovery, independent of the size of the proper motion error. ~~(We note that there could be a tiny bias $\ll 1$ SE in the $\ln(\sigma_{z,0}/200 \text{ km s}^{-1})$ qDF parameter, most likely due to insufficient numerical accuracy, but all the other model parameters, also those not shown in the figure, are very well behaved.)~~ Overall the standard errors on the recovered parameters are quite small (a few percent at most for 10,000 stars), which demonstrates that, if we perfectly knew the measurement errors, we still could get very precise constraints on the potential. The constraints also get tighter the smaller the proper motion error becomes. **We found that for $\delta\mu = 1 \text{ mas yr}^{-1}$ the precision of the recovered parameters reduce by \sim half compared to $\delta\mu = 5 \text{ mas yr}^{-1}$.**

The right column of panels in Figure 11 demonstrates the failure of our adopted likelihood approximation in the case of large distance modulus errors. The larger the $\delta(m - M)$, the wronger the recovered parameters become: The systematic biases can get many SEs large. We find however that in case of $\delta(m - M) \leq 0.2 \text{ mag}$ (if also $\delta\mu \leq 2 \text{ mas yr}^{-1}$ and a maximum distance of $r_{\text{max}} = 3 \text{ kpc}$, see Test 6.2 in Table 3) the parameters can still be recovered within 2 SEs. For most model parameters (except $\ln(\sigma_{z,0}/200 \text{ km s}^{-1})$, as shown in the figure, and $\ln(h_R/8 \text{ kpc})$) even $\delta(m - M) \leq 0.3 \text{ mag}$ still gives biases smaller than 2 SEs. This corresponds to a relative distance error of $\sim 10\%$. This encourages us that for smaller distance modulus errors we really could use our likelihood approximation in Equation (15), which is computationally cheaper than a proper treatment also on real data sets.

Underestimation of the proper motion error. **We found that in case we perfectly knew the measurement errors (and the distance error is negligible), the convolution of the model probability with the measurement errors gives precise and accurate constraints on the model parameters - even if the error itself is quite large.** Now we investigate what would happen if the quoted measurement errors, e.g. the proper motion errors, were actually smaller than the true errors. Figure 12 shows the case for two different stellar populations

-
-  **Author: rix Subject: Highlight** **Date: 15.09.15 12:52:09**
This is a very technical aspect: it should be summarized in 1-2 sentences; you neither have to provide code documentation, nor document effort. The reader wants the upshot.
-
-  **Author: rix Subject: Cross-Out** **Date: 15.09.15 12:46:46**
-
-  **Author: rix Subject: Highlight** **Date: 15.09.15 12:47:56**
This seems to be a (sensible) statement about the impact of the errors. Why is it under the heading of testing an approximation?
-
-  **Author: rix Subject: Highlight** **Date: 15.09.15 12:53:27**
That statement should be the last, concluding sentence of one of the previous sections. Then its fresh in the reader's mind, and does not need repeating.
-

and an error underestimation of 10% and 50%.

Overall the parameter recovery gets worse the larger the proper motion error and the stronger the underestimation. The relation between the bias due to error misjudgment and the size of the proper motion error seems to be linear.

For the recovery of the isochrone potential scale length b the hotness of the population does not matter (see lower left panel in Figure 12). The circular velocity $v_{\text{circ}}(R_{\odot})$ is, as always, better measured by cooler than by hotter populations (see upper left panel in Figure 12). We find that the recovery of the qDF parameters on the other hand is more strongly affected by the misjudgment of the velocity error for *cooler* stellar populations. The measured velocity dispersion is the convolution of the intrinsic dispersion with the measurement errors. If the proper motion error is underestimated, the deconvolved velocity dispersion is larger than the intrinsic velocity dispersion and the relative difference is bigger for a cooler population (see upper right panel for $\sigma_{z,0}$ in Figure 12). The intrinsic velocity dispersion is also cooler at larger radii than at smaller radii, therefore the deconvolved dispersion is overestimated more strongly at large R and the velocity dispersion scale length will be overestimated as well (see lower left panel for $h_{\sigma,z}$ in Figure 12). We got analogous results for the qDF parameters $\sigma_{R,0}$ and $h_{\sigma,R}$. The recovery of the tracer density scale length h_R is not affected by the misjudgment of velocity errors.

The most important and encouraging result from Figure 12 is, that for an underestimation of 10% the bias is still $\lesssim 2$ sigma **TO DO: can I say sigma???** - even for proper motion errors of almost 3 mas/yr.

3.5. The Impact of Deviations of the Data from the Idealized qDF

Our modelling approach assumes that each *MAP* follows a quasi-isothermal distribution function, qDF. In this Section we explore what happens if this idealization does not hold. ~~This could be, because even in the limit of perfectly measured abundances, MAPs do not follow a qDF. Or, even if they do follow a qDF, the finite abundance errors effectively mix different MAPs.~~ We investigate ~~both these issues~~ by creating mock data sets (Figure 13) that are drawn from two distinct qDFs of different temperature, and analyze the composite mock data set by fitting a single qDF to it. These results are illustrated in Figs. 14 and 15. Following the observational evidence, MAPs with cooler qDFs also have longer tracer scale lengths. In the first set of test, we choose qDFs of widely different temperatures and vary their relative fraction (dubbed “Examples 1a/b” in Figure 14 and Test 7 in Table 3); in the second set of tests (“Examples 2a/b” in Figure 15 and Test 7 in Table 3), we always mix mock data points from two different qDFs in equal proportion, but vary by how much the qDF’s temperatures differ.

Fig. 11.— Parameter recovery using the approximation for the measurement error convolved likelihood in Equation (15). All model parameters used to create the mock data sets analyzed for this figure are given as Test 6.2 in Table 3. The mock data sets in the left panels have only errors in line-of-sight velocity and proper motions, while the data sets in the right panels also have distance modulus errors, as indicated in the legends in the first row. The size of the error is color coded. The other panels plot the offset of the recovered model parameter to the true parameter vs. the relative standard error for two of the seven model parameters: the potential parameter $v_{\text{circ}}(R_{\odot})$ and qDF parameter $\sigma_{z,0}$. For data sets with proper motion error errors $\delta(m - M) \leq 3 \text{ mas yr}^{-1}$ Equation (15) was evaluated with $N_{\text{error}} = 800$ for $\delta(m - M) > 3 \text{ mas yr}^{-1}$ we used $N_{\text{error}} = 1200$. In the absence of distance errors Equation (15) gives unbiased results, for $\delta(m - M) \geq 3 \text{ mas yr}^{-1}$ (which corresponds in this test to $\delta v_{\text{max}} \lesssim 43$, see Equation (16)) however biases of several sigma [TO DO: can I say sigma??] are introduced as Equation (15) in only an approximation for the true likelihood in this case. [TO DO: rename σ_z to $\sigma_{z,0}$]

The first set of tests mimics a DF that has wider wings or a sharper core in velocity space than a qDF (Figure 13). The second test could be understood as mixing neighbouring MAPs due to too large bin sizes or abundance measurement errors.

It is worth considering separately the impact of the DF deviations on the recovery of the potential and of the qDF parameters.

We find from Example 1 that the potential parameters can be better and more robustly recovered, if a mock-data MAP is polluted by a modest fraction ($\lesssim 30\%$) of stars drawn from a much cooler qDF with a longer scale length, as opposed to the same pollution of stars drawn from a hotter qDF with a shorter scale length.

When considering the case of a 50/50 mix of contributions from different qDFs in Example 2, there is a systematic, but only small, error in recovering the potential parameters, monotonically increasing with the qDF parameter difference; in particular for fractional differences in the qDF parameters of $\lesssim 20\%$ the systematics are insignificant even for samples sizes of 20,000, as used in the mock data.

Overall, a cooler DF seems to always give tighter constraints on the circular velocity at the sun $v_{\text{circ}}(R_{\odot})$, because the rotation curve can be constrained easier if more stars are on near-circular orbits. But the recovered $v_{\text{circ}}(R_{\odot})$ does not necessarily have to be right. The hotter DFs give less tight constraints and are therefore more forgiving.

The recovery of the effective qDF parameters, in light of non-qDF mock data is quite intuitive: the effective qDF temperature lies between the two temperatures from which the mixed DF of the mock data was drawn; in all cases the scale length of the velocity dispersion fall-off, $h_{\sigma,R}$ and $h_{\sigma,z}$, is shorter, because the stars drawn from the hotter qDF dominate at

Author: rix Subject: Cross-Out Date: 16.09.15 07:00:31
Author: rix Subject: Inserted Text Date: 16.09.15 07:00:30
mock data drawn from a cooler DF always seem
Author: rix Subject: Inserted Text Date: 16.09.15 07:00:47
we found
Author: rix Subject: Inserted Text Date: 16.09.15 07:01:56
not always to be unbiased at the implied precision.

small radii, while stars form the cooler qDF (with its longer tracer scale length) dominate at large radii. The recovered tracer scale lengths, h_R vary smoothly between the input values of the two qDFs that entered the mix of mock data, with again the impact of contamination by a hotter qDF (with its shorter scale length in this case) being more important.

3.6. The Implications of Assuming a Potential Model which Differs from the Real Potential

We inspect if we can give constraints on the true potential, if our beliefs about the overall parametric form of the MW's potential are slightly wrong. We ignore deviations from axisymmetry and focus on a test case where the mock data was drawn from one axisymmetric potential ("MW14-Pot") and is then analysed using another axisymmetric potential family ("KKS-Pot"), that does *not* incorporate the true potential (compare the second and fourth panel in Figure 1). In the analysis we assume the circular velocity at the sun to be fixed and known and only fit the parametric potential form. The results are shown in Figure 16.

The reference potential parameters of the "KKS-Pot" in Table 1 were found by adjusting the 2-component Kuzmin-Kutuzov Stäckel potential by Batsleer & Dejonghe (1994) such that it generates radial and vertical force profiles similar to the "MW14-Pot" from Bovy (2015) (dotted gray lines in Figure 16). The analysis results from RoadMapping shown in Figure 16, red for a "hot" mock data MAP and blue for a "cool" MAP, give an comparable good or even better agreement with the true potential than the (by-eye) fit directly to the potential: especially the force contours, to which the orbits are sensitive, and the rotation curve are very tightly constrained and reproduce the true potential even outside of the observed volume of the mock tracers. This demonstrates that RoadMapping provides an optimal best fit potential within the capabilities of the parametric potential model.

The density contours are less tightly constrained than the forces, but we still capture the essentials: The "hot" MAP from Table 2 constrains the halo; especially at smaller radii it is equally good or better than the "cool" MAP. The "cool" MAP gives tighter constraints on the halo in the outer region and recovers the disk better than the "hot" MAP. This is in concordance with expectations as the "cool" MAP has a longer tracer scale length and is more confined to the disk than the "hot" MAP and therefore also probes the Galaxy in these regions better.

Overall the best fit disk is less dense in the midplane than the true disk.

Figure 17 compares the true qDF parameters with the best fit parameters. While tracer scale length and radial velocity dispersion profile are very well recovered, we misjudge the radial profile of the vertical velocity dispersion: $\sigma_{0,z}$ [TO DO: consistent] and $h_{\sigma,z}$ are both

Author: rix Subject: Inserted Text	Date: 16.09.15 07:03:03
Overall, we find that the potential inference is quite robust to modest deviations of the data from the assumed DF.	
Author: rix Subject: Inserted Text	Date: 16.09.15 07:04:00
a Gravitational Potential not from the Space of Model Potentials	
Author: rix Subject: Inserted Text	Date: 16.09.15 07:04:36
now explore what happens when	
Author: rix Subject: Inserted Text	Date: 16.09.15 07:04:43
are	
Author: rix Subject: Cross-Out	Date: 16.09.15 07:05:45
Author: rix Subject: Inserted Text	Date: 16.09.15 07:08:23
family, here	
Author: rix Subject: Inserted Text	Date: 16.09.15 07:08:27
,	
Author: rix Subject: Inserted Text	Date: 16.09.15 07:05:39
modelled considering potentials from only	
Author: rix Subject: Inserted Text	Date: 16.09.15 07:08:59
, here	
Author: rix Subject: Cross-Out	Date: 16.09.15 07:08:33
Author: rix Subject: Cross-Out	Date: 16.09.15 07:08:48
Author: rix Subject: Cross-Out	Date: 16.09.15 07:08:37
Author: rix Subject: Sticky Note	Date: 16.09.15 07:09:58
Do we have reason to believe that this very restrictive assumption does not qualitatively impact our upshot (quantitative differences are OK).	
Author: rix Subject: Inserted Text	Date: 16.09.15 07:06:30
S	
Author: rix Subject: Highlight	Date: 16.09.15 07:11:38
What does "reference" mean here exactly? Is this an independent exercise, to ask which parameters are expected when fitting potential to potential?	
Author: rix Subject: Cross-Out	Date: 16.09.15 07:20:46
Author: rix Subject: Inserted Text	Date: 16.09.15 07:20:28
We then run RoadMapping using these "inconsistent" families of gravitational families, and find a good fit to the data in configuration space (Fig. 18). [This used to be at the very end, even though its strikes me as the first thing to say; perhaps renumber Figures?]	
Author: rix Subject: Inserted Text	Date: 16.09.15 07:20:59
analysis for the potential	
Author: rix Subject: Inserted Text	Date: 16.09.15 07:13:02
Fitting infers a potential that in its actual properties resembles the input potential for the mock data as closely as possible, given the differences in functional forms.	
Author: rix Subject: Inserted Text	Date: 16.09.15 07:13:31
S,	
Author: rix Subject: Inserted Text	Date: 16.09.15 07:13:40
S,	
Author: rix Subject: Inserted Text	Date: 16.09.15 07:13:52
for this case.	
Author: rix Subject: Cross-Out	Date: 16.09.15 07:14:22

Fig. 14.— The dependence of the parameter recovery on degree of pollution and temperature of the stellar population. To model the pollution of a hot stellar population by stars coming from a cool population and vice versa, we mix varying amounts of stars from two very different populations, as indicated on the X -axis. The composite mock data set is then fit with one single qDF. The violins represent the marginalized likelihoods found from the MCMC analysis. *Example 1a* (*Example 1b*) in the left (right) panels mixes the “hot” (“cool”) MAP with the “cooler” (“hotter”) MAP in Table 2. All model parameters used to create the mock data are given in Test 7, *Example 1a*) & *b*) in Table 3. Some mock data sets are shown in Figure 13, first two rows, in the same colors as the violins here. We find, that a hot population is much less affected by pollution with stars from a cooler population than vice versa. [TO DO: rename $h_{\sigma R}$ to $h_{\sigma,R}$, σ_R to $\sigma_{R,\sigma}$ and analogous for z]

underestimated, which leads to a steeper profile and a lower dispersion around the sun. ~~This is a direct result of the surface density underestimation in the midplane, the corresponding lower vertical forces around the sun (see also Figure 16) and therefore lower vertical actions [TO DO: I have honestly no idea, if this is a proper explanation. In configuration space both models, original mock data set and best fit, have exactly the same radial dispersion and velocity profile.]. Figure 18 demonstrates that even though the misjudgment of the potential lead to biases in the qDF parameters, the model is still a very good fit to the data.~~

4. Discussion and Summary

Recently implementations of action DF - based modelling of 6D data in the Galactic disk have been put forth, in part to lay the ground-work fo Gaia (Bovy & Rix 2013; McMillan & Binney 2013; Piffl et al. 2014; Sanders & Binney 2015).

We present *RoadMapping*, an improved implementation of the dynamical modelling machinery by Bovy & Rix (2013), to recover the potential and orbit distribution function of stellar MAPs within the Galactic disk. In this work we investigated the capabilities, strengths and weaknesses of *RoadMapping* by testing its robustness against the breakdown of some of its assumptions - for well defined, isolated test cases using mock data. Overall the method works very well and reliable, also if there are small deviations of the model assumptions from the real world galaxy.

Fig. 15.— The dependence of the parameter recovery on the difference in qDF parameters of a 50%/50% mixture of two stellar populations and their temperature. Half of the star in each mock data set in *Example 2a* (*Example 2b*) was drawn from the "hot" ("cool") qDF in Table 2, and the other half drawn from a "colder" ("warmer") population that has $X\%$ smaller (larger) $\sigma_{R,0}$ and $\sigma_{z,0}$ and $X\%$ larger (smaller) h_R . Each composite mock data set is then fitted by a single qDF and the marginalized MCMC likelihoods for the best fit parameters are shown as violins. The model parameters used for the mock data creation are given as Test 7, *Example 2a*) & *b*) in Table 3. Some mock data sets are shown in figure 13, last two rows, where the distributions have the same colors as the corresponding best fit violins here. By mixing MAPs with varying difference in their qDF parameters, we model the effect of bin size in the $[\text{Fe}/\text{H}]-[\alpha/\text{Fe}]$ plane when sorting stars into different MAPs : The smaller the bin size, the smaller the difference in qDF parameters of stars in the same bin. We find that the bin sizes should be chosen such that the difference in qDF parameters between neighbouring MAPs is less than 20%. [TO DO: rename $h_{\sigma R}$ to $h_{\sigma R}$, σ_R to $\sigma_{R,0}$ and analogous for z]

4.1. Improved Computational Speed for Application to Larger Data Sets

RoadMapping applies a full likelihood analysis and is statistically well-behaved. It allows for a straightforward implementation of different potential model families and a flexible number of free fit parameters in potential and qDF. It also accounts for selection effects by using full 3D selection functions (given some symmetries). *RoadMapping* is an asymptotically normal, unbiased estimator and the precision of parameter recovery increases by $1/\sqrt{N}$ with the number of stars.

Large data sets in the age of Gaia require more, and more accurate, likelihood evaluations for more flexible models. To be able to deal with these increased computational demands and explore larger parameter spaces, we sped up the code by combining a nested grid approach with MCMC and by faster action calculation using the Stäckel (Binney 2012) interpolation grid by Bovy (2015). ~~Especially accurately determining the likelihood normalisation will be of crucial importance for large data sets. The nested grid approach automatizes the search for the optimal normalisation integration ranges ("fiducial qDF") and start position for the MCMC walkers, which helps the MCMC to converge fast and to reduce biases due to insufficient accuracy.~~ However, application of *RoadMapping* to millions of stars simultaneously with acceptable accuracy will still be a task for supercomputers and calls for even more improvements and speed-up in the fitting machinery.

Author: rix Subject: Cross-Out Date: 16.09.15 07:28:00

The discussion should not have numbered subsections; it's the distillation. I suggested alternatives below.

Author: rix Subject: Inserted Text

Date: 16.09.15 07:26:48

improved(84 Computational Speed=)

Author: rix Subject: Cross-Out Date: 16.09.15 07:26:07

said this before; the reader wants the upshot

4.2. Modelling Sensitivity to Properties and Unaccounted Imperfections of the Data Set

Choice of observation volume.

We found that the *position* of the survey volume matters little, in the sense that there are no regions in the Galaxy that contain intrinsically stars on manifestly more diagnostic orbits than others. Closer to the disk and at smaller Galactocentric radii it is only the increased number of stars that will lead to tighter constraints. Concerning the *shape* of the survey volume, a large radial and vertical coverage is best. In the axisymmetric case ϕ -coverage doesn't matter. Making a volume cut for stars that lie around R_0 but at larger ϕ , could therefore improve the results, if their measurements are very uncertain. MAPs of different scale length and temperature probe different regions of the Galaxy (Bovy & Rix 2013). But there is no easy rule of thumb for which survey volume and stellar population which potential and DF parameter is constrained best.

Selection function misjudgment. Surprisingly, RoadMapping seems to be very robust against misjudgments in the selection function of the data. The reason for this robustness could be, that missing stars in the data set do not affect the connection between a star's velocity and position, which is given by the potential. A lot of information about the potential profile is stored in the rotation curve - but even when not including measurements of tangential velocities in the analysis, small misjudgments of the incompleteness do not affect the potential recovery.

That we reproduce the qDF equally well, could be due to the symmetry of our assumed incompleteness profiles around the sun. We investigated a decrease in knowledge of the data completeness in distance from the sun and Galactic plane. Our test with the radial incompleteness profile could be understood as a decreasing detection rate due to the lower apparent brightness of stars at larger distances. The test with the planar incompleteness profile could mimic a misjudgment of the dust obscuration within the Galactic plane. Both effects would show the same symmetries as tested in this work.

This result is encouraging for future studies, but nevertheless surprising as it was previously believed that knowing the (spatial) selection function very precisely is of large importance for dynamical modelling (Rix & Bovy 2013).

Measurement errors. Properly convolving the likelihood with measurement errors is computationally very expensive. By ignoring positional errors and only including distance errors as part of the velocity error, we can drastically reduce the computational costs. For stars within 3 kpc from the sun this approximation works well for distance errors of $\sim 10\%$ or

Author: rix Subject: Cross-Out Date: 16.09.15 07:28:59

Author: rix Subject: Cross-Out Date: 16.09.15 07:33:40

Author: rix Subject: Inserted Text Date: 16.09.15 07:30:25
Properties of the data set.

Author: rix Subject: Inserted Text Date: 16.09.15 07:33:31
We could show that RoadMapping can provide potential and qDF parameters estimates that are very accurate (i.e. unbiased) and precise in the limit of large data sets, as long as the modelling assumptions are fulfilled. We also found that the location of the survey volume matters little. At given sample size, the volume over which the data are sampled also matters little, if the modelling assumptions are fulfilled.

Author: rix Subject: Inserted Text Date: 16.09.15 07:28:52

Author: rix Subject: Sticky Note Date: 16.09.15 07:34:49
Here, I tried to compactify the information on the sample properties.

Author: rix Subject: Cross-Out Date: 16.09.15 07:34:18

Author: rix Subject: Inserted Text Date: 16.09.15 07:34:07
, because in the axisymmetric regime the angular coverage does not matter.

Author: rix Subject: Cross-Out Date: 16.09.15 07:39:37

Author: rix Subject: Inserted Text Date: 16.09.15 07:41:09
(c.f. Rix and Bovy 2013)

Author: rix Subject: Inserted Text Date: 16.09.15 07:40:26
We speculate that this is because

Author: rix Subject: Cross-Out Date: 16.09.15 07:41:23

Author: rix Subject: Highlight Date: 16.09.15 07:39:06
This paragraph should be 1 or 2 sentences, following the first paragraph on "Sample/Data Properties".
This -- at the moments -- reads to be quite confusing. I don't quite get what the "upshot" is; there is technical detail on N_{error} [enough to say it's expensive]; and, as noted earlier, I don't understand why the error convolution for a nearby data point needs to know about data_{far}max.

smaller. The number of MC samples needed for the error convolution using MC integration scales by $N_{\text{error}} \propto (\delta v_{\text{max}})^2$ with the maximum velocity error at the edge of the sample. If we did not know the true size of the proper motion measurement errors perfectly, we can only reproduce the true model parameters to within $\lesssim 2$ sigma [TO DO: Can I say sigma???] [TO DO: Check???] as long as we do not underestimate it by more than 10% and for proper motion errors $\lesssim 2 \text{ mas yr}^{-1}$.

4.3. Data Deviations from the Modelling Assumptions about the Distribution Function and the Potential

Deviations from the qDF Assumption. Our modelling is founded on the assumption, that we can identify *a priori* sub-components of the Galactic disk that follow a qDF (e.g. by considering *MAPs*). There are two reasons why any chosen sub-sample of star (here a *MAP*) may not be well described by any qDF. Either, because nature is more complex, or because even if perfect *MAPs* would be well described by qDFs finite abundance errors would mix *MAPs*. We have considered both cases.

In Example 1 in §3.5 we investigated how well we can recover the potential, if this assumption was not perfectly satisfied, i.e. the *MAPs* true DF does not perfectly follow a qDF. We considered two cases: a) a hot DF, that has less stars at small radii and more stars with low velocities than predicted by the qDF (reddish data sets in Figure 13), or b) a cool DF that has broader velocity dispersion wings and less stars at large radii than predicted by the qDF (bluish data sets). We find that case a) would give more reliable results for the potential parameter recovery.

If we assumed that the distribution of stars from one *MAP* is caused by radial migration away from the initial location of star formation, it would more likely that the qDF overestimates the true number of stars at smaller radii than underestimating it at larger radii. [TO DO: Is this actually a sensible argument??]

Following this, focusing the analysis especially on hotter *MAPs* could be an advisable way to go in the future, if there is doubt that the stars truly follow the qDF.

Another critical point is the binning of stars into *MAPs* depending on their metallicity and α abundances. Example 2 in §3.5 could be understood as a model scenario for decreasing bin sizes in the metallicity- α plane when sorting stars in different *MAPs*, assuming that there is a smooth variation of qDF within the metallicity- α plane and each *MAP* indeed follows a qDF. We find that, in the case of 20,000 stars in each bin, differences of 20% in the qDF parameters of two neighbouring bins can still give quite good constraints on the potential parameters.

We compare this with the relative difference in the qDF parameters in the bins in Figure 6 of Bovy & Rix (2013), which have sizes of $[Fe/H] = 0.1$ dex and $\Delta[\alpha/Fe] = 0.05$ dex. It seems that these bin sizes are large enough to make sure that $\sigma_{R,0}$ and $\sigma_{z,0}$ of neighbouring MAPs do not differ more than 20%. Figure 14 and 15 suggest that especially the tracer scale length h_R needs to be recovered to get the potential right. For this parameter however the bin sizes in Figure 6 of Bovy & Rix (2013) might not yet be small enough to ensure no more than 20% of difference in neighbouring h_R . This is especially the case in the low- α ($[\alpha/Fe] \lesssim 0.2$), intermediate-metallicity ($[Fe/H] \sim -0.5$) MAPs. The above is valid for 20,000 stars per MAP. In case there are less than 20,000 stars in each bin the constraints are less tight and due to Poisson noise one could also allow larger differences in neighbouring MAPs while still getting reliable results.

Gravitational Potential beyond the Parameterized Functions Considered. In the long run *RoadMapping* should incorporate a family of gravitational potential models that can reproduce the essential features of the MW's true mass distribution. While our fundamental assumption of the Galaxy's axisymmetry is at odds with the obvious existence of non-axisymmetries in the MW, we will not dive into investigating this implications in the scope of this paper. Instead we test how a misjudgment of the parametric potential form affects the recovery by fitting a potential of Stäckel form (Batsleer & Dejonghe 1994) to mock data from a different potential family with halo, bulge and exponential disk. The recovery is quite successful and we get the best fit within the limits of the model. However, even a strongly flattened Stäckel potential component has difficulties to recover the very flattened mass distribution of an exponential disk. This leads to misjudgment of the qDF parameters describing the vertical action distribution, $\sigma_{z,0}$ and $h_{\sigma,z}$. As the qDF parameter $\sigma_{z,0}$ corresponds to the physical vertical velocity dispersion at the sun, a comparison with direct measurements could be a valuable cross-checking reference. [TO DO: This might not be true. For isochrone and Staackel potential I get this behaviour, but not for the MW14-Pot!!! Might be, because it's not separable??? Check!!!] In case of as many as 20,000 stars we should therefore already be able to distinguish between different potential models. The advantage of using a Stäckel potential with *RoadMapping* is firstly the exact and fast action calculation via the numerical evaluation of a single integral, and secondly that the potential has a simple analytic form, which greatly speeds up calculations of forces and frequencies (as compared to potentials in which only the density has an easy description like the exponential disk). A superposition of several simple Kuzmin-Kutuzov, Stäckel components can successfully produce MW-like rotation curves (see Batsleer & Dejonghe (1994), Famaey & Dejonghe (2003) and Figure 16) and one could think of adding even more components for more flexibility, e.g. a small roundish component for the bulge.

they used a superposition of action-based DFs to describe the overall stellar distribution at once: a superposition of qDFs for cohorts in the thin disk, a single qDF [TO DO: CHECK] for the thick disk stars and an additional DF for the halo stars. Taking proper care of the selection function requires a full likelihood analysis and the calculation of the likelihood normalisation is computationally expensive. Piffl et al. (2014) choose to circumvent this problem by directly fitting a) histograms of the three velocity components in eight spatial bins to the velocity distribution predicted by the DF and b) the vertical density profile predicted by the DF to the profiles by Jurić et al. (2008). The vertical force profile of their best fit mass model nicely agrees with the results from Bovy & Rix (2013) for $R > 6.6$ kpc. The disadvantage of their approach is, that by binning the stars spatially, a lot of stellar information is not used.

Sanders & Binney (2015) have focussed on understanding the abundance-dependence of the DF, relying on a fiducial potential. They developed extended distribution functions, i.e. functions of both actions and metallicity for a superposition of thin and thick disk, each consisting of several cohorts described by qDFs, a DF for the halo, a functional form of the metallicity of the interstellar medium at the time of birth, and a simple prescription for radial migration. They applied a full likelihood analysis accounting for selection effects and found a best fit for the eDF in a fixed fiducial potential by Dehnen & Binney (1998) to the stellar phase-space and metallicity [TO DO: CHECK] data of the Geneva-Kopenhagen Survey (GS) (Nordström et al. 2004; Holmberg et al. 2009) and the stellar density curves by Gilmore & Reid (1983). Their best fit predicted the velocity distribution of SEGUE G dwarfs quite well, but had biases in the metallicity distribution, which they accounted to being a problem with the SEGUE metallicities.

4.5. On the Assumption of Axisymmetry

The key assumption in our modelling, as well as in the approaches by Piffl et al. (2014) and Sanders & Binney (2015) described above, is the overall axisymmetry of Galaxy's potential and DF. This has the convenient advantage, that actions are conserved in axisymmetric potentials and can be calculated straightforward via the "Stäckel Fudge" by Binney (2012) and/or a single integration (in the case of separable potentials). Of course the Galactic disk is in reality not axisymmetric and actions are not conserved: Spiral arms in the disk and the Galactic bar lead to angular momentum exchange and therefore radial migration of stars, i.e. the orbit on which the stars were born on are modified (Minchev et al. 2011; Kawata et al. 2014). Apart from these obvious non-axisymmetries in the Galaxy, the disk itself is not smooth, as there is lot of sub-structure, streams and moving groups within the disk. A famous example is the Arcturus moving group, for which Navarro et al. (2004) found

that the stars might have their origin in a disrupted satellite. Spiral arms, the stirring of the Galactic bar and the disk sub-structure will undoubtedly affect our modelling with *RoadMapping*. How strong this effect will be and if the modelling can still work, needs to be investigated in detail in future work, e.g. by trying to recover the potential in N-body simulations. But as actions are conserved under adiabatic changes of the potential Binney & Tremaine (2008), and the vertical action under radial migration [TO DO: REF], there is some hope, that the modelling could still work.

The ultimate goal would be to theoretically describe those non-axisymmetries and sub-structures in terms of DFs in action/angle-abundance space. We see the current axisymmetric modelling approaches as intermediate step to this goal: Dehnen (1998) described the disk's overall stellar distribution as a smooth background distribution superimposed with sub-structure; the axisymmetric DFs used and to be found by *RoadMapping* and similar approaches could be treated as this smooth background. Firstly, this smooth background DF could help to actually find and identify the disk substructure in action space (see e.g. Sellwood (2010); Klement et al. (2008) for similar approaches to find disk substructure, which then helps to find DF descriptions. Secondly, and because simple superposition of action-based DFs is possible (see e.g. [TO DO: REF (see Payel's hint)]), the substructure DFs could then be directly added to the background DF and incorporated in the modelling. In other words, modelling the Galaxy together with its non-axisymmetries and substructure could be approached as applying perturbations to an axisymmetric equilibrium model. And *RoadMapping* will help finding this equilibrium model.

Such a Galaxy model will be also important in the meantime: Many studies of Galaxy structure and evolution use orbits as tracers and therefore require a reliable fiducial potentials to turn stellar positions and velocities into orbits. And as long as we are as far away from realistic Galaxy models as we are now, the axisymmetric case will need to be our reference.

5. Acknowledgments

[TO DO]

The authors thank Glenn van de Ven for the idea of using Kuzmin-Kutuzov Stäckel potentials in this case study.